Available online at www.sciencedirect.com

ScienceDirect

journal homepage: www.elsevier.com/locate/he

Optimization of hydrogen production via toluene steam reforming over Ni–Co supported modified-activated carbon using ANN coupled GA and RSM

Hamdya Sabrina Mohidin Yahya, Tariq Abbas, Nor Aishah Saidina Amin *

Chemical Reaction Engineering Group (CREG), School of Chemical & Energy Engineering, Faculty of Engineering, Universiti Teknologi Malaysia (UTM), 81310, Johor Bahru, Malaysia

HIGHLIGHTS

- ANN-GA and RSM techniques were used to design and optimize H_2 production via SRT.
- RSM based on central composite design (CCD) was applied to investigate SRT process.
- ANN model was coupled with Genetic Algorithm (GA) to optimize SRT process parameters.
- ANN with R^2=0.95 and RMSE=4.09 predicts better than RSM with R^2=0.87 and RMSE=6.92.
- ANN-GA proven as better method than RSM in data fitting and prediction of H_2 yield.

GRAPHICAL ABSTRACT

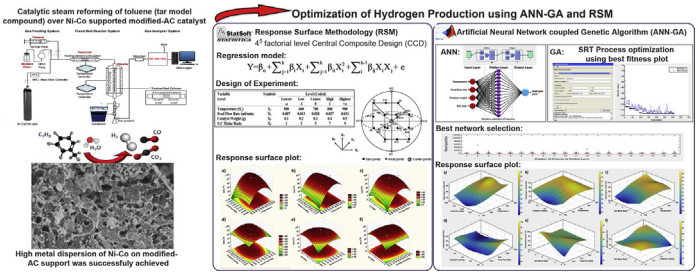

ARTICLE INFO

Article history:
Received 29 December 2019
Received in revised form
29 April 2020
Accepted 4 May 2020
Available online xxx

Keywords:
Artificial neural network-genetic algorithm (ANN-GA)
Response surface methodology (RSM)
Steam reforming of toluene
Activated carbon

ABSTRACT

Hydrogen (H_2) is a clean fuel that can be produced from various resources including biomass. Optimization of H_2 production from catalytic steam reforming of toluene using response surface methodology (RSM) and artificial neural network coupled genetic algorithm (ANN-GA) models has been investigated. In RSM model, the central composite design (CCD) is employed in the experimental design. The CCD conditions are temperature (500–900 °C), feed flow rate (0.006–0.034 ml/min), catalyst weight (0.1–0.5 g) and steam-to-carbon molar ratio (1–9). ANN model employs a three-layered feed-forward back-propagation neural network in conjugation with the tangent sigmoid (tansig) and linear (purelin) as the transfer functions and Levenberg-Marquardt training algorithm. Best network structure of 4-14-1 is developed and utilized in the GA optimization for determining the optimum conditions. An optimum H_2 yield of 92.6% and 81.4% with 1.19% and 6.02% prediction error are obtained from ANN-GA and RSM models, respectively. The predictive capabilities of the two models are evaluated by statistical parameters, including the coefficient of determination (R^2) and root mean square error (RMSE). Higher R^2 and

* *Corresponding author.*
E-mail addresses: noraishah@cheme.utm.my, profnoraishah@yahoo.com (N.A.S. Amin).
https://doi.org/10.1016/j.ijhydene.2020.05.033

Please cite this article as: Yahya HSM et al., Optimization of hydrogen production via toluene steam reforming over Ni–Co supported modified-activated carbon using ANN coupled GA and RSM, International Journal of Hydrogen Energy, https://doi.org/10.1016/j.ijhydene.2020.05.033

Nickel-cobalt
Hydrogen

lower RSME values are reported for ANN-GA model ($R^2 = 0.95$, RMSE = 4.09) demonstrating the superiority of ANN-GA in determining the nonlinear behavior compared to RSM model ($R^2 = 0.87$, RMSE = 6.92). These results infer that ANN-GA is a more reliable and robust predictive steam reforming modelling tool for H_2 production optimization compared to RSM model.

Abbreviations, nomenclature and units

Alphabetic symbols

C_7H_8	Toluene
Co	Cobalt
CO	Carbon monoxide
CO_2	Carbon dioxide
Co_3O_4	Cobalt (II, III) oxide
CoO	Cobalt (II) oxide
e	error term
H_2	Hydrogen
H_2O	Water
H_2O_2	Hydrogen peroxide
k	number of factors studied in the experiment
N_2	Nitrogen
Ni	Nickel
$NiCo_2O_4$	Nickel dicobalt (III) oxide
NiO	Nickel oxide
p-value	probability value
R^2	Coefficient of determination
X_1	Parameter related to temperature
X_2	Parameter related to feed flow rate
X_3	Parameter related to catalyst weight
X_4	Parameter related to steam-to-carbon ratio
X_i and X_j	Independent variables for the studied factors
Y	Predicted response

Abbreviations

3D	Three-dimensional
AC	Activated carbon
ACP	Hydrogen peroxide-modified activated carbon
ANN	Artificial neural network
ANN-GA	Artificial neural network coupled genetic algorithm
ANOVA	Analysis of variance
BET	N_2 adsorption-desorption by multi-points Brunauer-Emmet-Teller method
BP	Backpropagation
CCD	Central Composite Design
DOE	Design of experiments
FESEM	Field emission scanning electron microscopy
FID	Flame ionization detector
GA	Genetic algorithm
HPLC	High performance liquid chromatography
ICDD PDF-2 #	International Center for Diffraction Data Powder Diffraction File-2 number
IUPAC	International Union of Pure and Applied Chemistry
LM	Levenberg-Marquardt
MLP	Multi-layered perceptron
MSE	Mean square error
OVAT	One-variable-at-a-time
RMSE	Root mean square error
RSM	Response surface methodology
S/C ratio	The ratio of steam-to-carbon
SRT	Steam reforming of toluene
TCD	Thermal conductivity detector
WGS	Water gas shift
XRD	X-ray powder diffraction

Nomenclature

APD	Average pore diameter, nm
FFR	Feed flow rate, ml/min
$F^{in}_{Toluene}$	Inlet molar flow rates of toluene, mmol/min
$F^{out}_{H_2}$	Outlet molar flow rates of hydrogen, mmol/min
P/P_o	Relative pressure
S_{BET}	Specific surface area calculated by multi-points Brunauer-Emmet-Teller method, m^2/g
S_{mic}	Micropore surface area from t-plot y-intercept, m^2/g
T	Temperature, °C
V_t	Total pore volume, cm^3/g
W_{cat}	Catalyst weight, g
Y_{H_2}	Yield of H_2, %

Greek letters

β_o	constant coefficient
β_i	linear interaction regression coefficients
β_{ii}	quadratic interaction regression coefficients
β_{ij}	second-order interaction regression coefficients

Introduction

Hydrogen (H_2) has attracted considerable attention as the most promising energy carrier of the future to replace global dependencies on conventional fossil fuels. H_2 plays an important role as a sustainable fuel due to its high energy content and conversion efficiency with zero carbon emission [1]. According to the International Energy Agency, the global annual demand for H_2 energy has increased more than threefold since 1975 due to the rapid development of fuel cell technologies other than being used as feedstock for various

Please cite this article as: Yahya HSM et al., Optimization of hydrogen production via toluene steam reforming over Ni–Co supported modified-activated carbon using ANN coupled GA and RSM, International Journal of Hydrogen Energy, https://doi.org/10.1016/j.ijhydene.2020.05.033

industrial production [2]. However, extreme dependence on nonrenewable fossil fuel in H_2 production leaves a large carbon footprint to the H_2 manufacturing processes [3]. Nevertheless, due to the formation of tar, the green H_2 production technologies that utilize renewable biomass resources in the gasification process are facing major obstacles in the commercial scale. Tar is the unavoidable carbonaceous by-product during thermal conversion of biomass that consists of polycyclic aromatic hydrocarbon mixtures. The formation of tar could lower the gasification performances and increase process maintenance cost due to serious hazards associated with process equipment downstream and catalyst deactivation [4]. Hence, removal of tar is a critical issue that needs to be resolved for waste remediation and H_2 production.

Among available tar removal techniques, catalytic steam reforming is the most effective technique for converting tar to H_2 since the process can substantially reduce tar concentration and convert tar into valuable gases [5,6]. Toluene has been selected as tar model compound in this study as it represents major stable aromatic structure in complex tar compositions [4]. Nickel (Ni)-based catalysts are most commonly used in catalytic steam reforming of toluene (SRT) due to its high activity, low cost and easy regeneration [7]. High activity of Ni-based catalysts is attributed to the ability of Ni to activate the C–C and C–H bonds in the tar functional group structure. Conversely, Ni-based catalyst tends to suffer from deactivation due to the carbon formation during SRT. Cobalt (Co)-based catalysts are also considered as a promising candidate for steam reforming of tar and tar model compounds. The presence of Co^{2+} species promoted dehydrogenation reaction [8] and C–C bond breaking [9] that facilitated steam reforming reactions. Thus, it enhanced the water gas shift (WGS) reaction and reduced the formation of carbon on the catalyst [10]. Takise et al. [11] described that Co supported $La_{0.7}Sr_{0.3}AlO_{3-d}$ catalyst had higher catalytic stability in SRT compared to Ni supported catalyst provided by the redox properties and Co metal anchoring effect with its oxide support. Despite the excellent stability characteristic, lower catalytic activity was demonstrated by Co compared to Ni supported catalyst in the initial reaction before the catalyst deactivated. For this reason, different strategies have been investigated for Ni-based catalysts with the aim to increase the catalytic activity and stability, including the alloying of Ni catalyst with secondary metal (i.e., Co) and the modification of catalyst support [12,13].

Supported bimetallic catalytic systems are more favorable due to enhanced catalytic activity and higher stability compared with the monometallic counterparts [14–18]. In particular, bimetallic Ni–Co supported catalysts demonstrated superior catalytic performance in steam reforming of biomass tar model compounds such as phenol [19,20] and toluene [21]. Higher catalytic performance as compared to the bimetallic Ni–Co catalyst in relation to activity, stability and coke resistance is attributed by the promotive effect of Co addition to Ni catalysts. According to Li et al. [21], the addition of Co onto NiCo phyllosilicate@CeO_2 hollow spheres catalyst exhibited excellent catalytic activity and stability in SRT owing to the synergistic effect of Ni–Co solid solution alloy. The alloy improved carbon resistant property with better sintering resistance than Ni-catalysts. Other than the selection of active metal, catalytic support material is a key factor in designing an efficient steam reforming catalyst since it influences catalytic activity in reaction due to the variation in surface area and acid-base properties. Typical support material used for Ni-based catalysts for tar elimination includes dolomite [5,22], olivine [23,24] or metal oxides such as alumina [25,26] and magnesium oxide [27]. Nevertheless, the disadvantages of these support materials, such as easily eroded, metal sintering due to small surface area or susceptible to catalyst deactivation, significantly limit these options.

The characteristic of a good support material includes large specific surface area, unique pore structure and large adsorption capacity [28]. Among support materials available, biomass-derived activated carbon (AC) has demonstrated higher resistance to coke deposition than solid acid catalyst due to its neutral and weak-base properties [29–32]. In fact, carbon-based catalysts have been reported for the conversion of tar for industrial application [33]. AC is a low-cost material that has well-developed pore structural properties, high specific surface area and tunable surface chemistry (i.e., surface functional group) [34,35]. Generally, the physicochemical characteristics of AC depends on biomass precursor material and activation process. These properties can be improved further by tuning the textural and morphological features using surface modification technique to achieve high metal impregnation onto the AC surface [36,37]. The highly porous textural structures would facilitate the reactant molecule transport into the internal surface of catalyst to decrease catalyst deactivation by carbon formation [4]. The standard method for modifying AC surface is with oxidizing agents, such as hydrogen peroxide, where the porosity properties of AC can be improved through pore generation. Shen et al. [38] reported that the hydrogen peroxide-modification technique is able to improve the surface area of bamboo carbon to enhance metal adsorption ability. This method is considered as an environment-friendly technique compared to using nitric acid as the oxidizing agent.

Besides catalytic performance, the most important criterion to be considered in catalytic SRT for the production of H_2 is the optimization of the reaction variables. The determination of the most effective process conditions will maximize the reactant utilization of toluene for efficient H_2 production. Proper selection of variables such as temperature, feed flow rate, catalyst weight and steam-to-carbon (S/C) ratio may directly influence the selectivity of the desired product [21,24,39,40]. Numerous studies related to the process optimization of H_2 production have been reported using the classical single variable optimization by changing one variable at a time (OVAT). However, it is time-consuming, incurs high experimental cost and does not depict the interaction between different input variables [41,42]. Hence, the real affecting parameters related to the process variables may not be achieved. This approach could also lead to misinterpretation of results. Statistical methods or data analysis tools have gained much attention in modelling and process optimization to circumvent the shortcomings of OVAT.

Response surface methodology (RSM) and artificial neural network coupled genetic algorithm (ANN-GA) techniques are widely used for optimization [43–49]. The advantages of these techniques are that it assesses the relationship between the

Please cite this article as: Yahya HSM et al., Optimization of hydrogen production via toluene steam reforming over Ni–Co supported modified-activated carbon using ANN coupled GA and RSM, International Journal of Hydrogen Energy, https://doi.org/10.1016/j.ijhydene.2020.05.033

response and the independent variables, as well as evaluates the interaction of different input variables either in combination or independently [50–53]. In addition, these methods are considered as both time-saving and cost-effective since the required number of experiments are significantly less. RSM is a set of advanced statistical and mathematical methods that develop empirical models for process optimization and modelling. This method utilizes second-order polynomial regression analysis in a specified region of the independent variables to acquire the optimum values of independent variables for best responses. RSM is a powerful statistical analysis tool that is suitable in modelling complex multivariate processes where a response is influenced by multiple variables and the aim is to optimize this response [54]. Nevertheless, due to its ability to learn from observations and draw conclusions through generalization and predictive modelling behavior of complex nonlinear systems, ANN has emerged as a more versatile and superior modelling tool in process optimization compared to RSM.

ANN are computational and sophisticated mathematical models inspired by the simulation of biological phenomena that are well known for their extreme ability to learn and classify data. ANN consists of a massively interconnected network structure involving numerous simple processing elements capable of performing the parallel computation for data processing [55]. ANN can be optimized more precisely by using GA as the optimization tool. GA is the adaptive heuristic search algorithms for optimization on the basis of Darwinian principle of genetic evolution on the concept of "survival of the fittest" and employs genetic operators such as selection, mutation and crossover to find optimum solution of problem. The main application of the hybrid of ANN-GA is that ANN is utilized to build predictive models and predict the relationships between different data through adjustable parameters that can be trained, whereas, GA must be used to minimize (or maximize) the global search and to obtain feasible solutions with a known fitness function [56]. The prediction of ANN-GA model relies mainly on the training of the structured network [57].

Only limited studies employing RSM and ANN-GA as an effective modelling and optimization tool in catalytic SRT for H_2 production [56,58–61] are available. Toluene, as a model compound of tar (biomass gasification waste), has been chosen as the feed for producing H_2 in steam reforming. Also, the use of AC derived from palm kernel shell as the catalyst support in this study promotes the maximum utilization of biomass waste generated from palm oil mills. Palm kernel shell is one of the major wastes generated from oil palm mill and is conventionally being used as a boiler fuel for replacing diesel or charcoal [62]. The application of palm kernel shell-based AC as catalyst support is promising and has great potential in SRT reactions. This is due to higher porous characteristics than coconut shell [63] owing to the high lignin content and tunable surface properties.

Herein, the objective of this study is to develop effective RSM and ANN-GA models to optimize the catalytic SRT reaction over Ni–Co supported modified-AC catalyst. For the modelling part, RSM experimental design is selected to establish the regression model. The model involves four operating parameters (i.e., temperature, feed flow rate, catalyst weight and S/C ratio) as independent variables and H_2 yield as the only response. Meanwhile, the ANN model is developed to achieve the best neural network structure. Coupled with GA, the ANN-GA model is used for optimization of the SRT operating conditions to determine the maximum H_2 yield. The predictive capabilities and modelling efficiencies of the two models are evaluated and compared using statistical parameters, including coefficient of determination (R^2), root mean square error (RMSE) and various error analysis parameters. Moreover, the interaction effect of the independent variables with the response using the response surface plots are illustrated by the two models. Finally, the experimental yield is compared with the predicted values to determine the best predictive modelling tool for optimization of H_2 production.

Experimental

Materials and catalyst preparation of Ni–Co/ACP catalyst

The chemicals used in this study were nickel (II) nitrate hexahydrate (98% purity, Mërck), cobalt (II) nitrate hexahydrate (98% purity, Sigma-Aldrich), hydrogen peroxide (H_2O_2) (30% purity, Mërck) and analytical toluene (98%, QRëc). The activated carbon (AC) support was derived from palm kernel shell material (Multi Filter Sdn Bhd, Malaysia). Prior to the catalyst preparation, the AC support was modified using the H_2O_2 aging method by immersing AC particles (100 μm) in H_2O_2 solution (ratio = 1 g of AC:10 ml of H_2O_2) under continuous stirring at 5–20 °C for 6 h. Then, this sample was thoroughly washed and dried overnight at 110 °C and labelled as ACP. Ni–Co supported on ACP catalyst was successfully prepared by wet impregnation method of 10 wt% loading of each metal with constant stirring at 60 °C for 5 h. Sequentially, the slurry was oven-dried overnight at 110 °C, crushed and calcined at 500 °C for 4 h to obtain 10 wt% Ni-10 wt% Co/ACP catalyst. The synthesized catalyst was named as Ni–Co/ACP.

Characterization techniques

The physicochemical and structural properties of the synthesized catalysts were evaluated using nitrogen (N_2) adsorption-desorption (BET), X-ray powder diffraction (XRD) and field emission scanning electron microscopy (FESEM).

The BET analysis was analyzed by N_2 adsorption-desorption measurement of multi-points Brunauer-Emmet-Teller analysis using Thermo Scientific Surfer Analyzer (Thermo Fisher Scientific, Italy) to determine the textural properties of catalyst. BET specific surface area, pore diameter and volume were determined from the N_2 adsorption-desorption isotherm.

The XRD analysis was characterized using Rigaku SmartLab® X-ray diffractometer (Rigaku Corporation, Japan) measured over an angular range 2θ from 20° to 90° with a scanning rate of 1.2°/min via Cu-kα radiation (40 keV, 40 mA). The diffractometer was equipped with Ni-filtered Cu-kα radiation source (k = 1.54056 Å), operated at 40 kV and 200 mA.

The morphology of catalyst was investigated by FESEM analysis using Hitachi SU8020 integrated with the beam of X-Max^N by Oxford instrument optics and full control of probe

Please cite this article as: Yahya HSM et al., Optimization of hydrogen production via toluene steam reforming over Ni–Co supported modified-activated carbon using ANN coupled GA and RSM, International Journal of Hydrogen Energy, https://doi.org/10.1016/j.ijhydene.2020.05.033

current from 1 pA to more than 5 nA (Hitachi High-Technologies Corporation, Japan).

Catalytic activity test

Fig. 1 shows the schematic representation of the SRT experimental setup for H_2 production. The setup comprises three main systems, namely the gas feeding system, SRT reactor system and product gas analysis system. Gas feeding system involves toluene and water as the reactants that were fed into the subsequent system using a syringe pump with accuracy value ±2% of 0.118 ml/min (A99-E Syringe Pump, Razel® Scientific Instrument, USA) and a high performance liquid chromatography (HPLC) metering pump with accuracy value ±3% of 0.020 ml/min (LCP-01 Series I HPLC Pump, Scientific Systems, Inc., USA), respectively, which flowed into an evaporator that was set at the temperature of 150 °C. The N_2 gas serves as carrier gas with a constant flow rate of 15 ml/min that was regulated by a digital mass flow controller (Alicat Scientific, USA). The continuous fixed bed reactor of SRT was loaded with 0.3 g of catalyst supported by quartz wool placed vertically inside a split-tube furnace with ±5 °C temperature stability (Carbolite MTF 10/15/130, Germany). The reactor temperature was maintained using a programmable temperature controller. Then, outlet gas product composition was measured with gas chromatography (GC 6890N, Agilent Technologies) equipped with a flame ionization detector (FID) and thermal conductivity detector (TCD). The capillary columns used for the FID and TCD are Agilent GS-GasPro (Agilent, 60 m × 0.32; mm ID) and HP-Plot Q (Agilent, 40 m × 0.53; mm ID, 40 μm), respectively. The total flow rate of product gas was measured using a digital flow meter with accuracy value ±2% of output flow measurement reading (DFM-04 Model, PCI Analytics, India). The yield of H_2 (Y_{H_2}) was monitored as a response and calculated using Eq. (1) as follows:

$$Y_{H_2}(\%) = \frac{F^{out}_{H_2}}{18 \times F^{in}_{Toluene}} \times 100 \quad (1)$$

where $F^{out}_{H_2}$ and $F^{in}_{Toluene}$ are the outlet and inlet molar flow rates of H_2 and toluene, respectively. The stoichiometric ratio of water (H_2O) to toluene (C_7H_8) was established based on Eq. (2), which considering the SRT and WGS reactions, were also involved as in Eqs. (3) and (4) [26,64].

Steam reforming of toluene:

$$C_7H_8 + 14H_2O \rightarrow 7CO_2 + 18H_2 \quad (2)$$

$$C_7H_8 + 7H_2O \rightarrow 7CO + 11H_2 \quad (3)$$

Water gas shift (WGS):

$$CO + H_2O \rightleftharpoons CO_2 + H_2 \quad (4)$$

Response surface methodology (RSM)

Sequential statistics of four-factor five-level central composite design (CCD) was employed in the experimental design of optimization using STATISTICA 8.0 software (StatSoft, Inc., Tulsa, USA) to optimize several parameters affecting the catalytic SRT for H_2 production. The effect of significant parameters in SRT reaction including temperature (500–900 °C), feed flow rate (0.006–0.034 ml/min), catalyst weight (0.1–0.5 g) and S/C molar ratio (1–9) was studied at five experimental levels (−2 (α), −1, 0, +1, +2 (α)) as listed in Table 1. These variables are coded as X_1, X_2, X_3 and X_4, accordingly. Total of twenty-six (26) runs of experiment is required in this study where experimental points consist of sixteen star points ($\alpha = \pm 1$), eight axial points ($\alpha = \pm 2$) and two replicates at the center point ($\alpha = 0$), as elucidated and labelled with each run number in Fig. 2. The design of experiments (DOE) parameters for each run can be

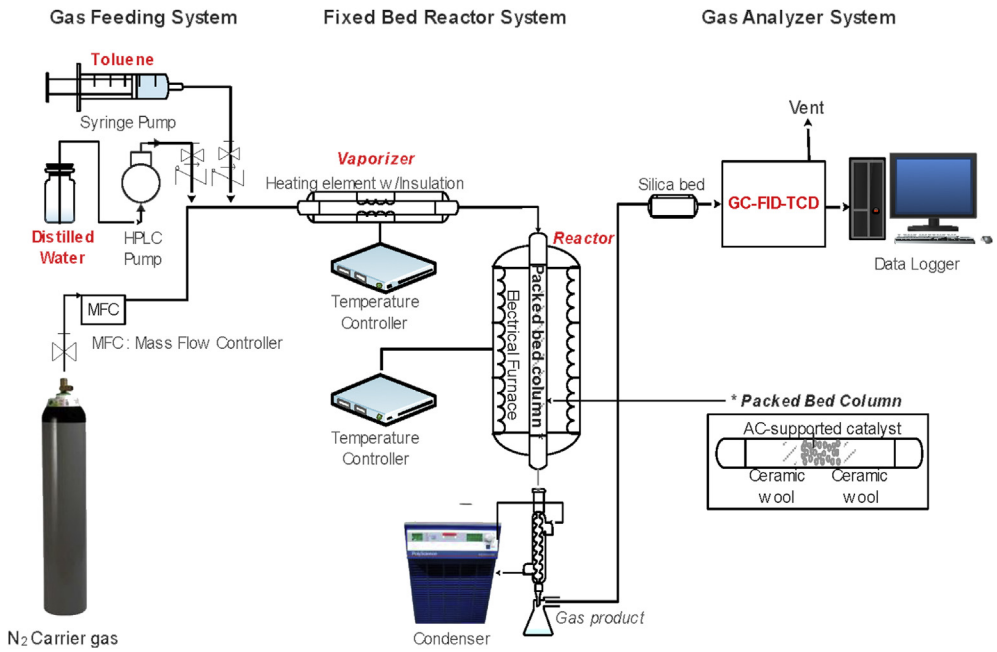

Fig. 1 – Experimental setup for catalytic steam reforming of toluene for H_2 production.

Please cite this article as: Yahya HSM et al., Optimization of hydrogen production via toluene steam reforming over Ni–Co supported modified-activated carbon using ANN coupled GA and RSM, International Journal of Hydrogen Energy, https://doi.org/10.1016/j.ijhydene.2020.05.033

Table 1 – Experimental parameters with the value for each level and response.

Independent Variables	Symbol (unit)	Coded Level	Level (Coded)				
			Lowest	Low	Center	High	Highest
			-α	−1	0	1	+α
Temperature	T (C)	X_1	500	600	700	800	900
Feed Flow Rate,	FFR (ml/min)	X_2	0.006	0.013	0.020	0.027	0.034
Catalyst Weight	W_{cat} (g)	X_3	0.1	0.2	0.3	0.4	0.5
S/C Molar Ratio	S/C	X_4	1	3	5	7	9

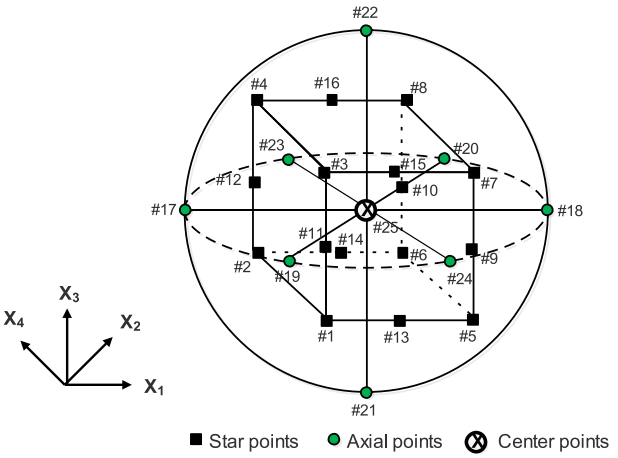

Fig. 2 – Diagram of four-factor five-level second-order central composite experimental design.

referred to in Table 4. The runs were carried out in duplicate and randomized manner to minimize systematic biases. Central points were used to evaluate the stability and reproducibility of the experimental results. Catalytic SRT performance was evaluated by analyzing the H_2 yield (Y_{H_2}) as the response. Experimental data obtained from the CCD model were subjected to the following quadratic model to predict the response function and estimate the coefficients by multiple regression analysis, as in Eq. (5) [65]:

$$Y = \beta_o + \sum_{j=1}^{k} \beta_i X_i + \sum_{j=1}^{k} \beta_{ii} X_i^2 + \sum_{i}^{k-1} \beta_{ij} X_i X_j + e \quad (5)$$

where Y is the predicted response, X_i and X_j are the studied factors chosen as the independent variables, β_o, β_i, β_{ii} and β_{ij}, represent the constant coefficient, linear, quadratic and second-order interaction regression coefficients, respectively. k is the number of factors studied in the experiment and e is the error term.

Analysis of variance (ANOVA) was used for the verification and adequacy of the model. The Fischer F-test was used to verify the statistical significance of the model [66]. The selection and rejection of the model terms were set with a confidence level of 95% on the probability value (p-values) and a significance level of 5%. This is followed by the representation of the response surface contour plot to demonstrate the interaction effects and individual impacts of the variables on the response. In addition, the coefficient of determination (R^2) was utilized to determine the fitness of the model. R^2 is the key parameter in model assessment that describes the percentage of variation with 1 as 100% of variation that can be described by the model and 0 as the total inability of a model to approximate the reforming reaction [67]. High value of R^2 closer to 1 indicates that the model provides the goodness of fit of the polynomial model to experimental data.

Three-dimensional (3D) response surface plots were plotted to visualize the interaction effect of the independent variables with the response and to determine the optimal condition of each variable for the catalytic SRT process. These plots were depicted by varying two variables, while other variables were kept at zero level. Also, the experimental values of the response were measured and the predicted values obtained from the model were evaluated. The coefficients of the equations and the ANOVA test were calculated and the respective response surface plots were illustrated accordingly.

Artificial neural network coupled genetic algorithm (ANN-GA)

ANN modelling

In order to construct an accurate and robust ANN model, it is necessary to consider the architecture of neural network. Other than that, the most important factors to be considered are the selection of the type of learning algorithm and transfer function to be used in the hidden and output layers, as well as the number of hidden neurons. In general, ANN structure was designed according to the multi-layered perceptron (MLP) type, which approximates nonlinear relationships existing between the dependent (output) and independent (input) variables. The ANN network is developed by assembling the training data, creating the neural network architecture, followed by training, testing, validation and simulation of network responses for new inputs. The development of network architecture and optimization of the process parameters were performed using the MATLAB 8.4 2014b™ software. In this research, the multi-layered feed-forward neural network comprises three layers, namely input, output and hidden layers. The input layers send signals to the artificial neurons in the hidden layer through an organization of variable weights to the output layer, as depicted in Fig. 3a [68]. The hidden layer is the intermediate layer that separates the layer of input and output, generated by a set of hidden neurons. The number of hidden layers is selected as one layer in this study as it is considered sufficient for most problems to avoid overfitting issues due to the application of more than one hidden layer [69]. Next, the number of neurons in hidden layer was determined by the trial and error method, where the hidden neurons were iterated to achieve optimum value. It is important to properly decide the number of hidden neurons to

Please cite this article as: Yahya HSM et al., Optimization of hydrogen production via toluene steam reforming over Ni–Co supported modified-activated carbon using ANN coupled GA and RSM, International Journal of Hydrogen Energy, https://doi.org/10.1016/j.ijhydene.2020.05.033

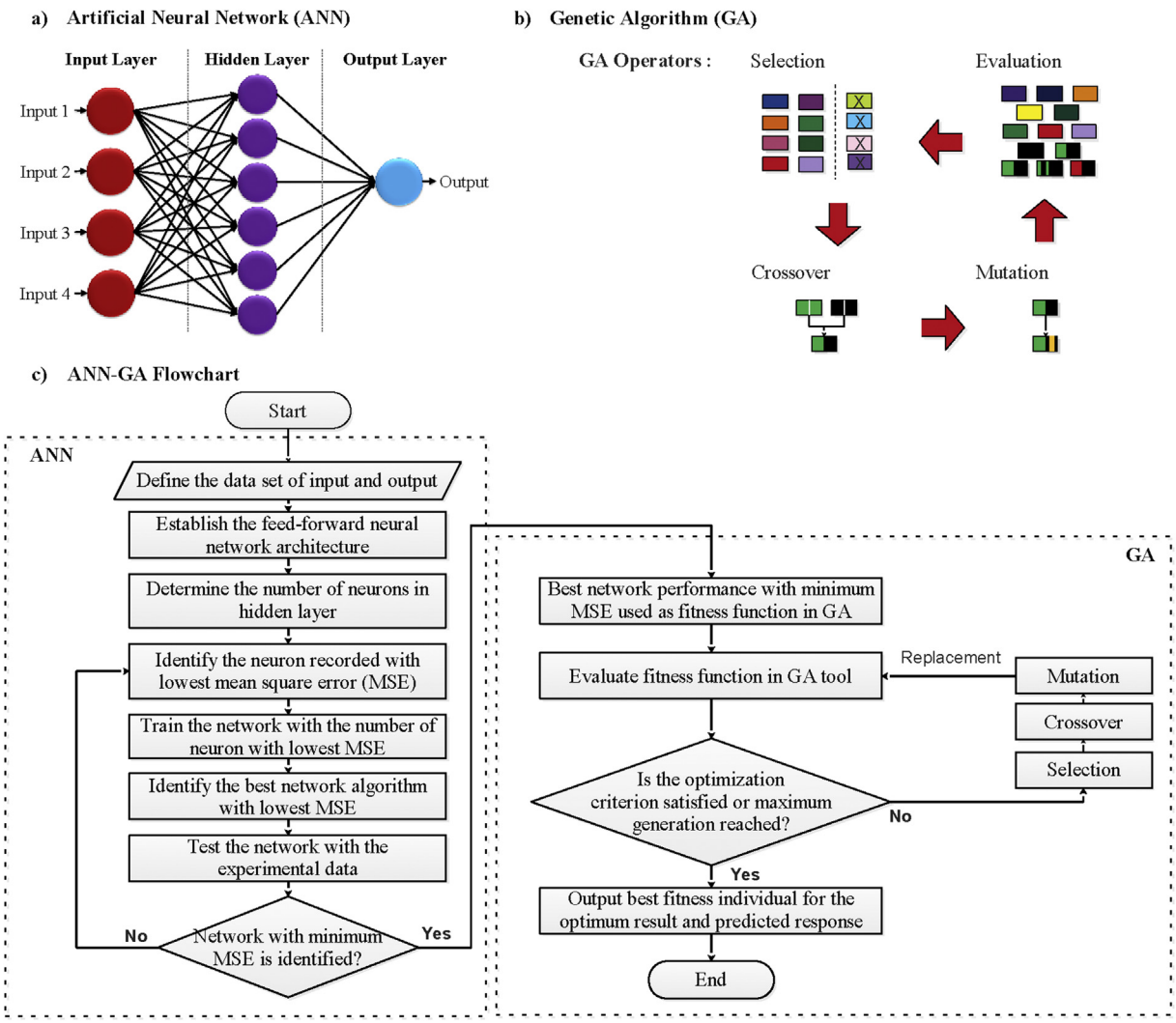

Fig. 3 – (a) Schematic diagram of the multi-layered perceptron architecture of ANN structure; (b) basis of GA operation; and (c) flow chart of integrating ANN with GA for H_2 production optimization via catalytic SRT.

avoid the "overfitted" and "underfitted" model. Typically, in cases of underfitted model, the number of hidden neurons is too few as compared with the complexity of the problem. However, the overfitted model will take place if an excessive number of hidden neurons are used since the generalization capability of the network will be degraded when the model is trained based on the training data only [70].

Backpropagation (BP) and Levenberg-Marquardt (LM) were selected as the learning algorithm and training function, respectively. The BP learning algorithm was employed to train the neural network structure as it is recommended by majority of researchers [67,71] because of its high reliability in function optimization and modelling [72]. The types of transfer function for the hidden and output layers are also essential because it significantly influences the learning rate or the overall performance of the neural network [73]. The nonlinear transfer function used in this study is the hyperbolic tangent sigmoid (tansig) in the hidden layers, whereas the linear (purelin) transfer function is used in output layer to convert the input signals into nonlinear output signals. The sigmoid function is mostly used in the BP neural network, with an output range from 0 to 1 [74]. The optimum value of the hidden layer is considered as the optimum performance for the ANN model, which is attained by a hidden neuron with the lowest MSE value. The mean square error (MSE) is typically used, as shown in Eq. (6) [75]:

$$\mathrm{MSE} = \frac{1}{N}\sum_{i=1}^{N}\left(Y_{\mathrm{ANN}} - Y_{\mathrm{Exp}}\right)^2 \quad (6)$$

where Y_{ANN} is the predicted output from ANN, Y_{Exp} is the experimental data and N is the number of samples. The best predicted algorithm is determined by the training algorithm with lowest error value. Hence, the lowest MSE was then recorded for the respective number of neurons and subsequently used in the training of the network to search for the network with the lowest MSE.

Optimization of ANN structure by GA

The best network structure obtained from ANN model was further used to determine the optimum conditions using the

Please cite this article as: Yahya HSM et al., Optimization of hydrogen production via toluene steam reforming over Ni–Co supported modified-activated carbon using ANN coupled GA and RSM, International Journal of Hydrogen Energy, https://doi.org/10.1016/j.ijhydene.2020.05.033

Genetic Algorithm Solver or 'ga – Genetic Algorithm' available in the Optimization toolbox (ver. 7.1) of MATLAB software by generating the best fitness plot for the response of H_2 yield [76]. The 'ga' function utilizes a kind of controlled elitist genetic algorithm that assigns fitness scaling and ranks each individual in an objective function space according to the dominance depth or degree of nondomination. The combination of ANN and the GA algorithms in a hybrid system is important to support the modelling and optimization simultaneously. The key features of GA are as follows: (a) it needs the scalar values only instead of the second- and/or first-order derivatives of the objective functions; (b) it is able to handle the nonlinear and noisy objective functions; (c) it conducts the global searches and hence it is highly expected to reach at or near the global optimum instead of local optimum values; and (d) it does not enforce preconditions on the objective functions, such as smoothness, differentiability and continuity. Due to these attractive features of GA, it is beneficial to be used in solving various optimization problems presents in chemical engineering [77]. Thus, the operating condition of catalytic SRT over Ni–Co/ACP catalyst is optimized using GA to achieve maximum H_2 production in this study.

The GA operates by altering the population of individual solutions repeatedly. The GA process involves the selection, crossover and mutation, which generates the "children" solutions from the "parent" or initial population that will subsequently be used for the next generation. The subsequent population will then evolve to the optimal solutions according to the specified fitness function [69]. Fig. 3b and 3c shows the basis of GA operation and the flow chart of integrating ANN with GA, respectively, for the process optimization of H_2 production via catalytic SRT to find the optimum conditions for H_2 yield response.

Results & discussion

Catalyst characterization

The most significant feature of AC materials is contributed by its textural properties as assessed by the N_2 adsorption-desorption isotherm plots (Fig. 4). The physisorption isotherms of untreated AC and modified ACP supports are classified as Type I isotherm with H4 shaped hysteresis loops according to the International Union of Pure and Applied Chemistry (IUPAC) classification. This type of isotherm consists of typical micropores and mesoporous structure [78]. As shown in Fig. 4, the adsorption takes place at a very low relative pressure (P/P_o) less than 0.02, and the slight rise in plateau from low to high relative pressure (P/P_o) at around 0.6 to 0.8 reveals highly porous structure with narrow pore size distribution [79]. Although the isotherm plot for modified ACP occur at higher P/Po compared to AC, almost no change was observed in the shape of isotherm plots for AC and ACP. This finding indicates that the support modification method is able to preserve the unique porous structure of the AC without affecting drastic rupture of its surface porosity and texture. The isotherm plot increment for ACP sample takes place due to the increase of surface area after the modification. Slight enlargement of the hysteresis loops of ACP ($P/P^o = 0.43$) compared to AC ($P/P^o = 0.48$) is attributed to the increase of pore size distribution and the presence of mesopores. The hysteresis loops of isotherm plots are generally associated with the capillary condensation that takes place in mesopore structures, and its shape represents specific pore structures. According to the IUPAC nomenclature [80], the presence of H4 hysteresis loops for both samples are ascribed to the characteristic of narrow slit-shaped pores, which were mostly in the range of micropore structure [81,82]. The detailed textural properties analysis of the isotherms for AC, ACP and Ni–Co/ACP catalysts are summarized in Table 2. The average pore diameter (APD) of AC and ACP is 2.12 and 1.83 nm, respectively. The specific surface area (S_{BET}) is determined by the multi-point Brunauer-Emmet-Teller method in the region of isotherm that is limited by the range of relative pressure P/P_o of 0.01–0.1. Hence, the adsorbed volume displays the BET surface area for AC and ACP is 684.29 and 738.92 m^2/g, respectively. These results infer that the H_2O_2-modification method generates a highly microporous structure of ACP.

On the other hand, an inverse observation of the isotherm plot for Ni–Co/ACP catalyst is obtained. The isotherm plot of ACP changes significantly from classical

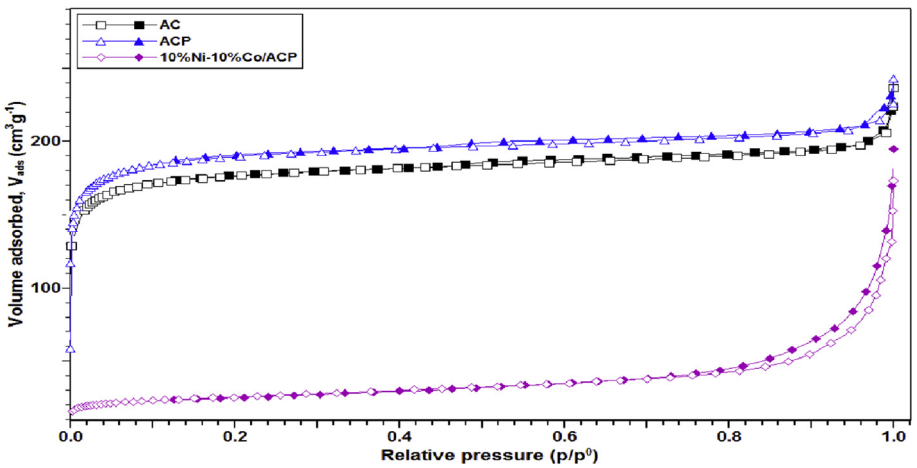

Fig. 4 – N_2 adsorption (open symbol)-desorption (closed symbol) isotherm of AC, ACP and Ni–Co/ACP catalysts.

Please cite this article as: Yahya HSM et al., Optimization of hydrogen production via toluene steam reforming over Ni–Co supported modified-activated carbon using ANN coupled GA and RSM, International Journal of Hydrogen Energy, https://doi.org/10.1016/j.ijhydene.2020.05.033

Table 2 – Textural properties of the AC, H_2O_2-modified AC (ACP) and Ni–Co/ACP samples.

Sample	S_{BET} (m^2/g)[a]	V_t (cm^3/g)[b]	APD[c] (nm)	S_{micro} (m^2/g)[d]
AC	684.29	0.32	2.12	632.86
ACP	738.92	0.42	1.83	674.38
10%Ni–10%Co/ACP	90.77	0.29	4.38	1.05

[a] S_{BET}:specific surface area by the multi-point Brunauer-Emmet-Teller method.
[b] V_t:total pore volume of pores at P/Po = 0.9999.
[c] APD:average pore diameter.
[d] S_{mic}:micropore surface area from t-plot y-intercept.

Type I to Type IV and the S_{BET} reduces for Ni–Co/ACP catalyst upon the Ni–Co metal impregnation onto the surface of ACP support. Total pore volume (V_t) of Ni–Co/ACP decreases to 0.2674 cm^3/g at a relative pressure $P/P_o = 0.9999$ with presence of H3 hysteresis loop inferring mesoporous material. Other researchers reported similar findings, which is lower specific surface area of metal-supported AC catalysts was observed compared to their parent AC support [83,84]. The decrement of specific surface area and pore volume for Ni–Co/ACP is probably attributed to the presence of small metal particles on the external surface and in the pore of modified ACP [85,86]. Modification of ACP support leads to high dispersion of Ni–Co metal particles.

In order to investigate the effect of metal loading on catalyst support, XRD characterization of the AC and Ni–Co/ACP samples are depicted in Fig. 5 in comparison with the reference peaks. As can be seen in Fig. 5, the AC support gives broad diffraction peaks at 2θ angles of 25.3° (002) and 43.62° (101) that could be assigned as amorphous and graphene or graphite. Yao Chen and coworkers have reported similar diffraction peaks for the graphene-AC catalyst [87]. In contrast, the Ni–Co/ACP catalyst displays diffraction peaks at 2θ = 37.01° (101), 43.14° (012), 62.67° (110), 75.36° (113), and 79.39° (202) of nickel oxide (NiO) (ICDD PDF-2# 01-078-4374) indicating the presence of the active phase of NiO on the catalyst. Also, the diffraction peaks of cobalt oxide at 2θ = 36.9° (111), 42.93° (200), 62.43° (220), 75.04° (311) and 78.91° (222) are observed, which designated as CoO phase (ICDD PDF-2# 01-070-2855). Two diffraction patterns of Co_3O_4 (ICDD PDF-2# 03-065-3103) and $NiCo_2O_4$ (ICDD PDF-2# 01-073-1702) phase at 36.9° (311) and 64.8° (400) are also recorded [88–90]. The detailed crystallinity information for AC and the Ni–Co/ACP catalyst corresponding to the facets of NiO, CoO, Co_3O_4 and $NiCo_2O_4$ are listed in Table 3.

FESEM micrographs of Ni–Co/ACP were obtained to investigate the surface morphology related to the porous structures as well as the active metal dispersion on the support, as shown in Fig. 6. It is observed that small Ni or Co particles were uniformly present on the external surface and inside the pore walls of ACP support, indicating that the Ni–Co/ACP catalyst exhibited a high dispersion of active

Table 3 – XRD analysis of the fresh sample of the Ni–Co/ACP catalyst.

	2θ (degree)	*hkl* indices	ICDD PDF-2 #
AC	25.30	002	01-075-2078
	43.62	101	
NiO	36.9	101	01-078-4374
	42.93	012	
	62.43	110	
	75.04	113	
	78.91	202	
CoO	36.9	111	01-070-2855
	42.93	200	
	62.43	331	
	75.04	220	
	78.91	311	
Co_3O_4	36.9	311	03-065-3103
	64.8	400	
$NiCo_2O_4$	36.9	311	01-073-1702
	64.8	400	

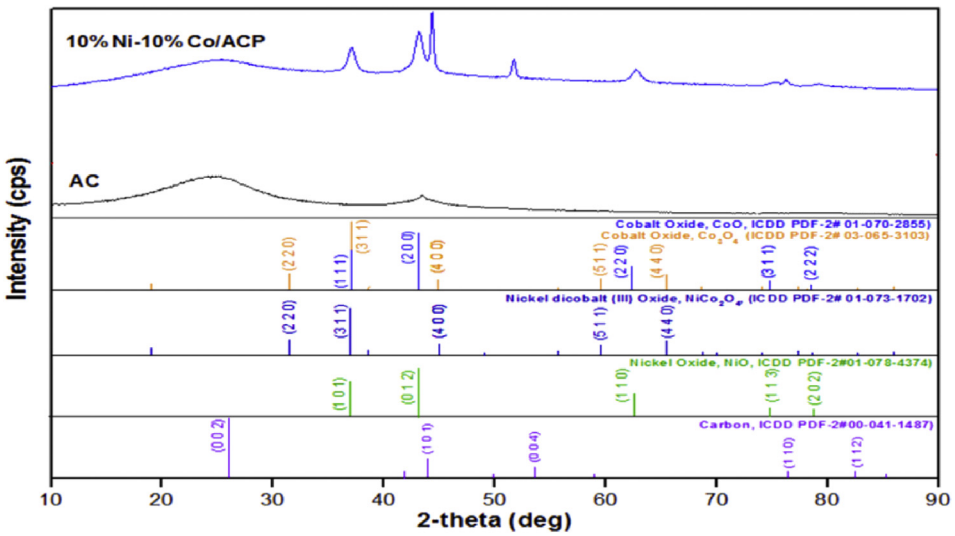

Fig. 5 – XRD spectra of AC and Ni–Co/ACP catalysts.

Please cite this article as: Yahya HSM et al., Optimization of hydrogen production via toluene steam reforming over Ni–Co supported modified-activated carbon using ANN coupled GA and RSM, International Journal of Hydrogen Energy, https://doi.org/10.1016/j.ijhydene.2020.05.033

Table 4 – SRT variables in central composite design (real and coded value) of four independent parameters with experimental and predicted responses by RSM and ANN models.

Run	Location	Actual variables (Coded values)				H_2 yield, Y_{H_2}		
		X_1 (T, °C)	X_2 (FFR, ml/min)	X_3 (W_{cat}, g)	X_4 (S/C)	Experimental	RSM Predicted Values	ANN-GA Predicted Values
1	Star	600 (−1)	0.013 (−1)	0.2 (−1)	3 (−1)	60.42	55.62	61.56
2	Star	600 (−1)	0.013 (−1)	0.2 (−1)	7 (+1)	64.37	60.88	62.82
3	Star	600 (−1)	0.013 (−1)	0.4 (+1)	3 (−1)	67.84	63.60	63.71
4	Star	600 (−1)	0.013 (−1)	0.4 (+1)	7 (+1)	70.33	67.72	62.96
5	Star	600 (−1)	0.027 (+1)	0.2 (−1)	3 (−1)	70.52	53.12	75.23
6	Star	600 (−1)	0.027 (+1)	0.2 (−1)	7 (+1)	60.71	59.75	54.13
7	Star	600 (−1)	0.027 (+1)	0.4 (+1)	3 (−1)	61.16	55.82	62.96
8	Star	600 (−1)	0.027 (+1)	0.4 (+1)	7 (+1)	58.63	61.32	64.73
9	Star	800 (+1)	0.013 (−1)	0.2 (−1)	3 (−1)	72.27	71.54	68.26
10	Star	800 (+1)	0.013 (−1)	0.2 (−1)	7 (+1)	68.14	71.18	65.23
11	Star	800 (+1)	0.013 (−1)	0.4 (+1)	3 (−1)	80.94	79.60	79.59
12	Star	800 (+1)	0.013 (−1)	0.4 (+1)	7 (+1)	88.86	78.12	94.50
13	Star	800 (+1)	0.027 (+1)	0.2 (−1)	3 (−1)	90.22	78.73	95.15
14	Star	800 (+1)	0.027 (+1)	0.2 (−1)	7 (+1)	73.55	79.75	70.88
15	Star	800 (+1)	0.027 (+1)	0.4 (+1)	3 (−1)	76.08	81.53	81.77
16	Star	800 (+1)	0.027 (+1)	0.4 (+1)	7 (+1)	78.92	81.41	75.88
17	Axial	500 (−α)	0.020 (0)	0.3 (0)	5 (0)	24.26	34.50	37.50
18	Axial	900 (+α)	0.020 (0)	0.3 (0)	5 (0)	80.40	70.50	75.94
19	Axial	700 (0)	0.006 (−α)	0.3 (0)	5 (0)	69.00	73.89	64.56
20	Axial	700 (0)	0.034 (+α)	0.3 (0)	5 (0)	79.22	74.68	69.15
21	Axial	700 (0)	0.020 (0)	0.1 (−α)	5 (0)	71.73	64.82	73.59
22	Axial	700 (0)	0.020 (0)	0.5 (+α)	5 (0)	75.19	74.45	74.38
23	Axial	700 (0)	0.020 (0)	0.3 (0)	1 (−α)	69.72	82.97	82.84
24	Axial	700 (0)	0.020 (0)	0.3 (0)	9 (+α)	86.96	81.08	75.99
25	Center	700 (0)	0.020 (0)	0.3 (0)	5 (0)	82.07	82.97	76.08
26	Center	700 (0)	0.020 (0)	0.3 (0)	5 (0)	83.86	82.97	76.08

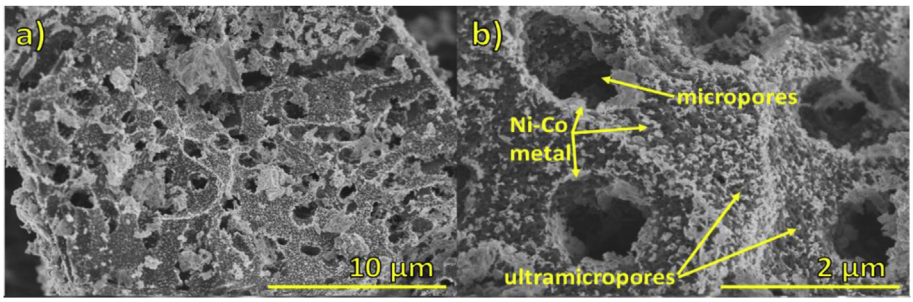

Fig. 6 – FESEM of Ni–Co/ACP catalyst at (a) 5000x and (b) 25000x magnification scale.

metal Ni–Co over ACP support. This finding is consistent with the aforementioned BET and XRD results of the catalyst. It can be suggested that H_2O_2-modification method has successfully improved porous structure by removing the impurities and inorganic compounds present on the carbon surfaces as well as in the pores. These findings concur with other investigations that reported the H_2O_2 modification on activated carbon leads to an increase of specific surface area of carbon support [38] and metal dispersion enhances with smaller metal particles [91]. In addition, the presence of micropore structures, observed under the magnification of 25000x (Fig. 6b), contributed to the increment of the microporous texture of the ACP support. It could be surmised the increment of the surface area and microporous properties has assisted the attachment of active metals onto the carbon surfaces.

Response surface methodology (RSM) modelling

Development of model equation

The experimental results reveal that H_2 yield is affected by temperature, feed flow rate, catalyst weight and S/C ratio. The second-order polynomial-regression model is designed by using selected input parameters and output response of Y_{H_2} (Eq. (7)). The quadratic regression equation displays empirical relationship between four independent variables and yield of H_2 in terms of coded forms. Table 4 tabulates 26 sets experiments required for analyzing the effect of selected parameters

Please cite this article as: Yahya HSM et al., Optimization of hydrogen production via toluene steam reforming over Ni–Co supported modified-activated carbon using ANN coupled GA and RSM, International Journal of Hydrogen Energy, https://doi.org/10.1016/j.ijhydene.2020.05.033

in catalytic SRT for H_2 production and its interactions using the CCD.

$$Y_{H_2} = -401.4 + 1.1X_1 - 301.5X_2 + 175.2X_3 + 11.8X_4 - 0.0X_1^2 - 44309.9X_2^2 - 111.4X_3^2 - 0.8X_4^2 + 3.5X_1X_2 - 0.1X_1X_3 + 0.0X_1X_4 + 490.8X_2X_3 - 94.2X_2X_4 - 1.4X_3X_4 \quad (7)$$

The regression equation infers the Y_{H_2} as a function of reforming temperature (X_1), feed flow rate (X_2), catalyst weight (X_3) and S/C ratio (X_4). The interdependent interaction of variables is displayed in the form of linear, square and two-way interaction of regression. Eq. (7) shows that the Y_{H_2} depends on linear interaction of X_1, X_2, X_3 and X_4 and square interaction with the parameter itself of X_1-to-X_1, X_2-to-X_2, X_3-to-X_3 and X_4-to-X_4. Eq. (7) also indicates the two-way interaction of regression between the parameters such as X_1-to-X_2, X_1-to-X_3, X_1-to-X_4, X_2-to-X_3, X_2-to-X_4 and X_3-to-X_4. The model demonstrates quadratic coefficient of feed flow rate (X_2) had the main adverse effect on H_2 production for its highest negative coefficient value. The positive sign in model indicates that increment of the variable will increase response value and negative sign will impose otherwise.

Analysis of variance (ANOVA)

ANOVA method was used to assess the adequacy and validity of the generated regression models. This is to determine the significant effect of SRT process variables to Y_{H_2} as well as to fit the second-order polynomial models to the experimental data. The pronounced results of ANOVA analysis for Y_{H_2} are provided in Table 5. F-value and p-value was used to determine the statistical significance of the model. Fischer (F) test describes the adequacy of model where it represents ratio of mean square due to regression to the mean square due to residual error. Higher F-value calculated than tabulated value and its corresponding p-value lower than 0.05 for the developed model infers that the parameters were considered significant. The parameters were considered insignificant if F-value is lower than the tabulated value or the p-value is greater than 0.05. ANOVA of regression model illustrates that the developed model is highly significant as evident from the calculated F-value (5.12) that exceeded the tabulated F-value for 95% confidence ($F_{0.05}$) (2.201) and its corresponding p-value (0.000). There is only 0.005% chance that the model's value could occur due to noise. Strong correlation between the predicted model and output factor is observed for the R^2 value (0.87) is higher than the acceptable value of 0.85 in RSM methodology. Hence, the obtained model provides a good estimation of the predicted response within the studied range.

Pareto analysis was used to elucidate the significance of each variable and its interactions on the measured response of Y_{H_2}. In Pareto chart, at 95% confidence level, variables are organized from maximum significance (lower *p*-values) to minimum significance (higher *p*-values). Fig. 7 illustrates the Pareto chart of independent variables with corresponding *p*-values for H_2 yield. It is apparent that temperature is the most significant variable with lowest *p*-value (<0.0001), followed by steam-to-carbon ratio. The significant influence of temperature on H_2 yield is attributed to the endothermic nature of steam reforming process [5,22].

Table 5 – Analysis of variance (ANOVA) for the response surface of linear and quadratic models of the hydrogen yield in catalytic steam reforming of toluene over Ni–Co/ACP catalyst.

Source	Sum of square	Degree of freedom	Mean square	F-value	*p*-value
Regression Model	3436.88	14	245.49	5.12	0.0000
Linear	2124.74	4	531.19	11.09	0.0000
X_1 - Temperature	1944.88	1	1944.88	40.59	<0.0001
X_2 – Feed flow rate	0.94	1	0.94	0.02	0.8914
X_3 – Catalyst weight	39.73	1	39.73	0.83	0.3820
X_4 – S/C ratio	139.19	1	139.19	2.90	0.1164
Square	1310.42	4	327.61	6.84	0.0000
X_1^2	1012.59	1	1012.59	21.13	0.0007
X_2^2	82.28	1	82.28	1.72	0.2168
X_3^2	21.66	1	21.66	0.45	0.5152
X_4^2	193.89	1	193.89	4.05	0.0694
2-Way Interaction	156.64	6	26.11	0.54	0.0000
X_1 X_2	94.14	1	94.14	1.96	0.1886
X_1 X_3	31.52	1	31.52	0.66	0.4345
X_1 X_4	0.01	1	0.01	<0.01	0.9896
X_2 X_3	1.89	1	1.89	0.04	0.8462
X_2 X_4	27.80	1	27.80	0.58	0.4622
X_3 X_4	1.28	1	1.28	0.03	0.8732
Residual Error	527.07	11	47.92		
Total	3963.95	25			

$R^2 = 0.87$, Total runs = 26 runs.

Please cite this article as: Yahya HSM et al., Optimization of hydrogen production via toluene steam reforming over Ni–Co supported modified-activated carbon using ANN coupled GA and RSM, International Journal of Hydrogen Energy, https://doi.org/10.1016/j.ijhydene.2020.05.033

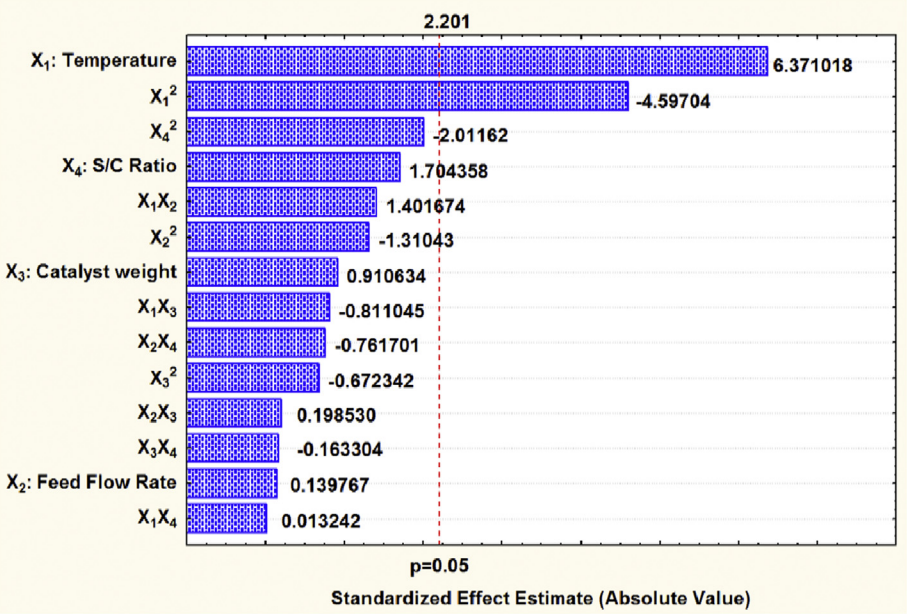

Fig. 7 – Pareto chart and p-value obtained from RSM.

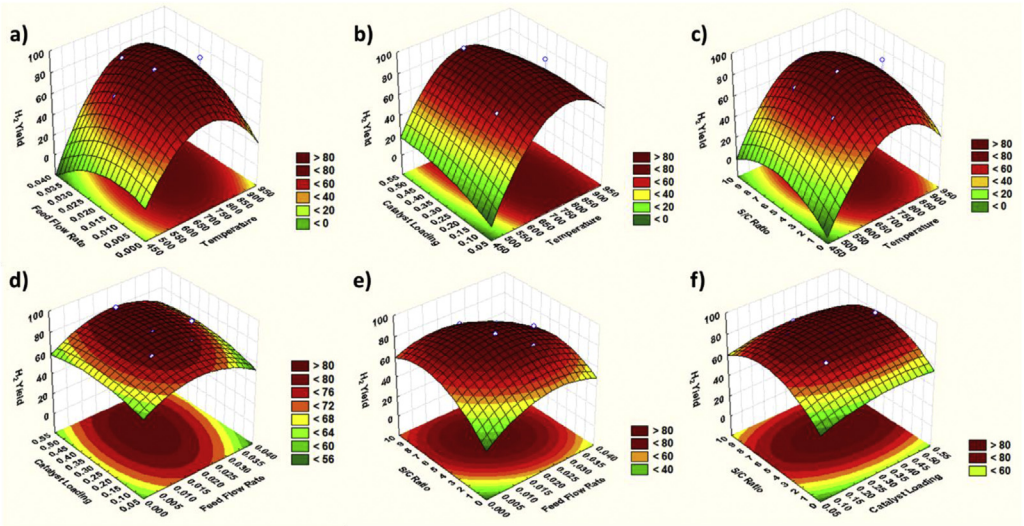

Fig. 8 – 3D response surface plot for Y_{H_2} and (a) temperature vs feed flow rate; (b) temperature vs catalyst weight; (c) temperature vs S/C ratio; and (d) catalyst weight vs feed flow rate; (e) S/C ratio vs feed flow rate; and f) S/C ratio vs catalyst weight.

Three-dimensional (3D) response surface plot

The mutual interaction between independent variables and H_2 yield is elucidated by the 3D response surface plots, as shown in Fig. 8 a-f. Fig. 8a displays the interactive effects of temperature and feed flow rate on H_2 yield. It can be seen from Fig. 8a that increasing feed flow rate causes H_2 yield to decrease at a lower temperature. This phenomenon could be ascribed to the decrease in residence time between catalyst surface and reactants [60]. However, with the increase in reaction temperature from 600 to 850 °C at a constant feed flow rate, H_2 yield increases. Maximum H_2 yield is obtained at lower feed flow rates and higher temperature. This finding is expected, since the increase in H_2 production is attributed to the endothermic nature of steam reforming reaction [60]. Hence, the surface plot elucidates that the interaction between temperature and feed flow rate significantly influences H_2 production in SRT.

Another significant interaction on the H_2 yield is catalyst weight and reaction temperature, as presented in Fig. 8b. At higher reforming temperature (>600 °C), H_2 yield increases with an increase in the catalyst weight. This enhancement in H_2 yield might be attributed to the increase in surface area of catalyst bed and the residence time of the reactants within catalyst bed [60,92].

Please cite this article as: Yahya HSM et al., Optimization of hydrogen production via toluene steam reforming over Ni–Co supported modified-activated carbon using ANN coupled GA and RSM, International Journal of Hydrogen Energy, https://doi.org/10.1016/j.ijhydene.2020.05.033

Fig. 8c depicts the interaction effect between reforming temperature and S/C ratio on H_2 yield. The guidance of surface plot elucidates that the interaction between temperature and S/C ratio substantially influences H_2 yield in output product gas. Both steam reforming temperature and S/C ratio favors H_2 yield production. From this result, it is clear that high H_2 yield is expected at high values of reforming temperature and S/C ratio [16,17,93].

Based on the surface response plot, the interaction between catalyst weight and feed flow rate contributes to significant interaction to the H_2 yield (Fig. 8d). Higher H_2 yield could be attained at a higher feed flow rate and higher catalyst weight. However, the value of H_2 yield begins to reduce with the increase of feed flow rate above 0.035 ml/min. The decrement of H_2 yield implies the effect of contact time is very crucial to ensure the promotion of the WGS reaction and to achieve sufficient energy required to overcome the activation energy barrier for the reaction [94]. The plots also portray that low H_2 yield could be obtained at higher feed flow rate due to insufficient contact time to promote WGS reaction. Similarly, low H_2 yield is also expected at lower feed flow rate due to high formation of reaction by-products. Hence, feed flow rate and catalyst weight need to be optimized in order to achieve the highest H_2 yield. The highest H_2 yield is observed at the feed flow rate of 0.020 ml/min and catalyst weight 0.30 g.

The interaction between S/C ratio and feed flow rate on H_2 yield is illustrated in Fig. 8e. As the S/C ratio increases, the reaction augments the desirable reaction in SRT, which favors higher H_2 yield due to the increment of water molecule in feed stream promoting the steam reforming and WGS reaction. At lower S/C ratio and feed flow rate, lower H_2 yield is observed. This could be attributed to the encapsulation of active metal sites on the catalyst surface due to coke formation and reverse WGS reaction [95].

Fig. 8f elucidates the interaction between S/C ratio and catalyst weight on H_2 yield. The guidance of the response surface plot exhibits that at a lower S/C ratio (0–2), the effect of catalyst weight is less significant. A higher amount of carbon in feed stream causes lower H_2 yield due to higher undesirable reactions, including carbon formation and reverse WGS reaction. High H_2 yield is observed as the S/C ratio and catalyst weight increase. From this result, it is clear that H_2 yield is favored at relatively higher reaction temperature and S/C ratio as the carbon formation and reverse WGS reaction is thermodynamically inhibited under these conditions implying endothermic reaction [93]. However, optimal values of feed flow rate and catalyst weight are desired since it directly affects the contact time between reactant and active metal sites of catalyst.

ANN-GA modelling

Development and training of the network

MATLAB 2014b™ (The Mathworks Inc.) software is used to develop the codes to design the ANN structure that comprises of multiple-input single-output neural network for the prediction of Y_{H_2}. Experimental results obtained from the DOE software of RSM are employed in developing the ANN architecture for the catalytic SRT as depicted in Fig. 9a. The number of neurons in the hidden layer is obtained by the iteration of

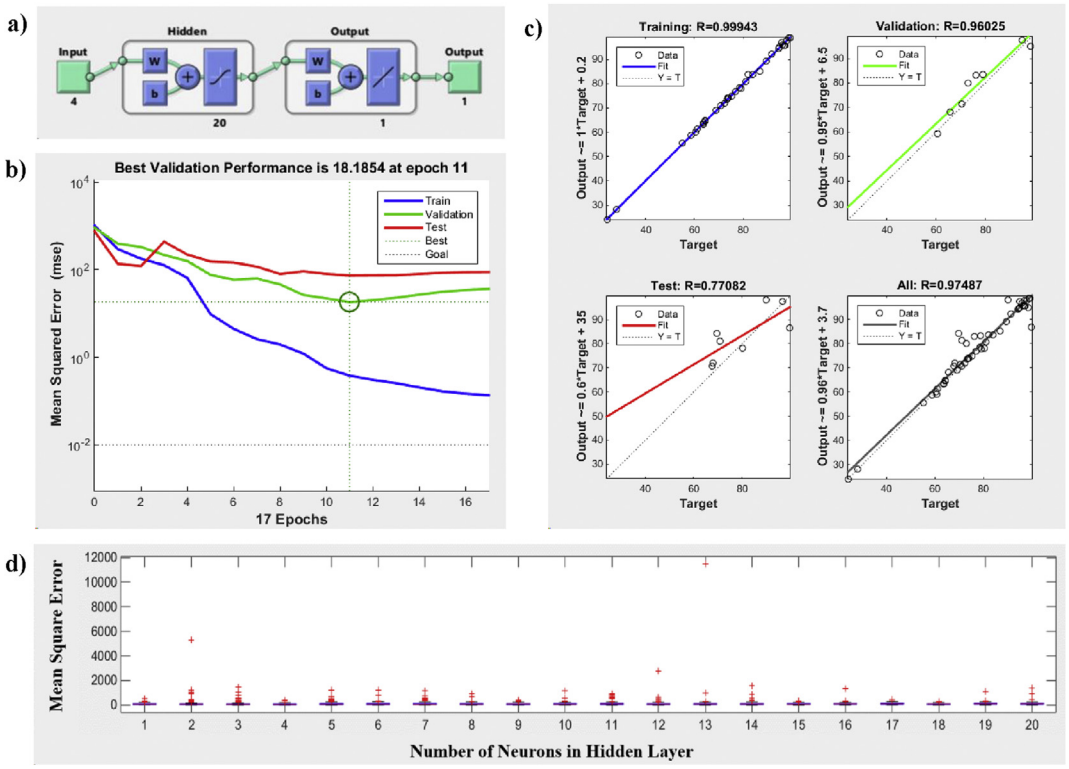

Fig. 9 – (a) ANN architecture topology with input, hidden (tangent sigmoid transfer function) and output layer (pure linear transfer function); (b) ANN training validation performance plot; (c) Regression of experimental vs predicted values in ANN model in each step; (d) Mean square error (MSE) for different number of neurons in the hidden layer (1-20) for H_2 yield (Y_{H_2}).

Please cite this article as: Yahya HSM et al., Optimization of hydrogen production via toluene steam reforming over Ni–Co supported modified-activated carbon using ANN coupled GA and RSM, International Journal of Hydrogen Energy, https://doi.org/10.1016/j.ijhydene.2020.05.033

network for the minimum value of MSE. 70% of the data is employed to train the network, whereas the remaining data are for validating and testing of the networks. Error minimization within the networks comprises of appropriate selection of the number of neurons in the hidden layer. The calculated network error is compared with the output continuously until the network reaches the minimum error by adjusting weights and biases. The learning cycle and maximum epoch are set at 0.5 and 100, respectively. In order to obtain the minimum MSE of the training network, the number of hidden neurons is tested for the corresponding MSE starting from the lowest value. Subsequently, this process produces the optimum neurons with lowest MSE value. The ANN training validation performance plot and the regression of experimental vs predicted values in ANN model in each step were plotted, as in Fig. 9b and 9c. The MSE plot for different number of neurons in hidden layer (1-20) for the response of H_2 yield is depicted in Fig. 9d. It is observed that the lowest MSE is obtained with 14 neurons for the H_2 yield. The trained network with 14 hidden neurons is found to yield the minimum value of MSE of 82.12 which occurs at the 5th network. Therefore, the best network structure of 4-14-1 is used for process optimization which represents 4 inputs in the first layer, followed by 14 neurons in the hidden layer and one output in the last layer.

GA process optimization

Process optimization uses GA solver by applying the optimized network of ANN model as the input to generate the best fitness function for the optimization problem [96], as depicted in Fig. 10a. The Y_{H_2} component to be maximized is negated in the vector-valued fitness function separately since 'ga' minimizes all the objectives. Experimental ranges are set as bounds on the four input variables and fifty individuals within the bounds are chosen in the initial population. Table 6 enlists the numerical parameter values used in the GA options for the optimization runs. In this optimization, the rank method is applied for the fitness scaling, whereas stochastic uniform is utilized for the selection method in order to stipulate how the GA chooses parents for the next generation. From the 50 numbers of population size, two of them are elite counts and are used in the next generation, whereas 80% of the remaining population is employed for the crossover reproduction and 20% is utilized for the mutation reproduction.

Table 6 – Computational parameters of genetic algorithm used in the process optimization for hydrogen yield.

Computational parameters	Values
Population size	50
Elite count	2
Crossover fraction	0.80
Number of generations	400
Fitness scaling function	Rank fitness scaling
Selection function	Stochastic uniform
Crossover function	Constraint dependent
Mutation function	Constraint dependent mutation function
Direction for migration	Forward with migration fraction set at 0.2
Nonlinear constrain algorithm	Augmented Lagrangian

The best fitness plot can assist the process operator to fix the input control variables in order to obtain the locally optimum points of selected operating parameters with respect to Y_{H_2}. Hence, the best fitness plot for Y_{H_2} is attained after 311 iterations, as displayed in Fig. 10b. At the optimum conditions, the predicted Y_{H_2} is 93.7%, which corresponds to the following parameters: temperature, 700 °C; feed flow rate, 0.034 ml/min; catalyst weight, 0.1 g; and S/C molar ratio, 1.

Interaction between the independent variables and hydrogen yield by ANN

The graphical representation of the interaction between studied variables and Y_{H_2} in SRT over Ni–Co/ACP catalyst obtained from ANN modelling is illustrated in Fig. 11a–f. The interaction effects in ANN modelling graphs exhibited greater prediction accuracy as compared to the response surface plots of RSM modelling, as in Fig. 8. This can be contributed by the approximation ability of ANN through nonlinearity of the system, while RSM only belongs to a second-order polynomial. The relationship between temperature and feed flow rate on Y_{H_2} is presented in Fig. 11a. It can be seen that H_2 production is more favorable at high temperature and medium feed flow rate. The interaction is more insignificant at low temperature and medium flow rate since steam reforming reaction has high probability of reaching its thermodynamic equilibrium at higher temperatures as it is an endothermic reaction. Hence, high temperature is the main contributor to promote WGS reaction and H_2 production.

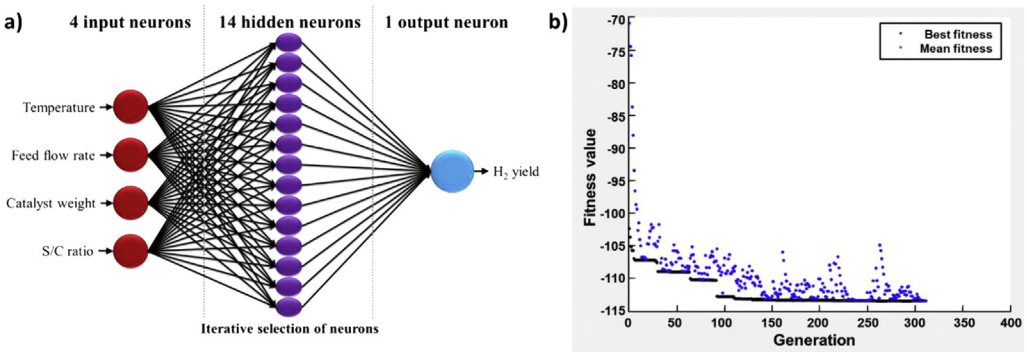

Fig. 10 – (a) Optimized ANN structure for GA optimization and prediction of H_2 yield in SRT; and (b) Best fitness plot for H_2 yield (Y_{H_2}) obtained from ANN-GA model.

Please cite this article as: Yahya HSM et al., Optimization of hydrogen production via toluene steam reforming over Ni–Co supported modified-activated carbon using ANN coupled GA and RSM, International Journal of Hydrogen Energy, https://doi.org/10.1016/j.ijhydene.2020.05.033

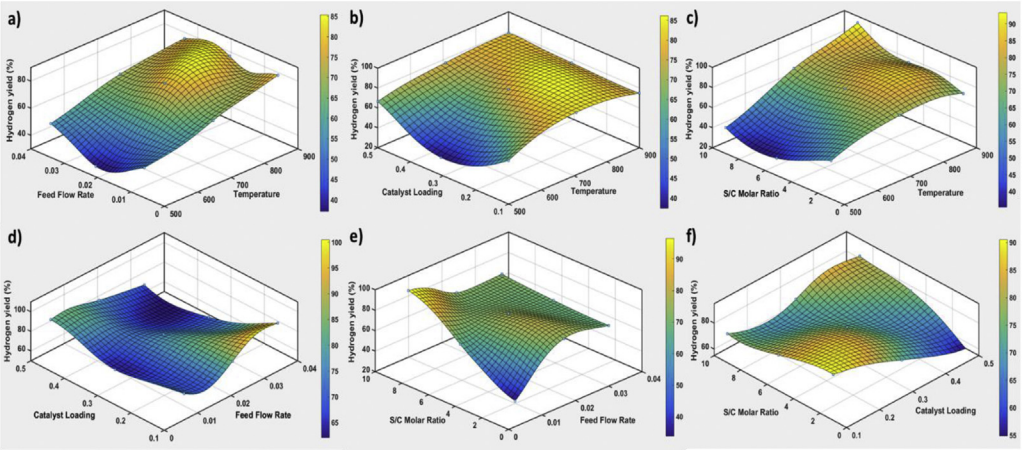

Fig. 11 – Response surface plots of H_2 yield based on ANN modelling as a function of: (a) temperature (X_1) and feed flow rate (X_2); (b) temperature (X_1) and catalyst weight (X_3); (c) temperature (X_1) and S/C ratio (X_4); (d) feed flow rate (X_2) and catalyst weight (X_3); (e) S/C ratio (X_4) and feed flow rate (X_2); and (f) S/C ratio (X_4) and catalyst weight (X_3).

Based on Fig. 11b, it is clearly shown that high Y_{H_2} is obtained by increasing the temperature. Low Y_{H_2} is observed at a lower temperature and medium catalyst weight. However, only slight variation of Y_{H_2} is observed on the variation of catalyst weight after the temperature exceeded 600 °C. This is in good agreement with the H_2 production reported by Basu et al. [93], where the Y_{H_2} remained almost unchanged after reaching a certain temperature. In fact, Y_{H_2} may decrease slightly when the temperature was increased further due to the reverse WGS reaction and the Boudouard reaction.

Fig. 11c illustrates the response surface plot of the interaction between temperature and S/C molar ratio on H_2 production. It can be observed that medium S/C molar ratio (~3) and high reaction temperature (>700 °C) are favored for higher H_2 production. Higher H_2 yield is more favorable to occur at high temperatures due to the endothermic nature of steam reforming reaction [30]. The formation of CO was higher at low temperature as a result of the decomposition of reactant and reverse WGS reaction. Moreover, at high S/C molar ratio, WGS reactions become more favorable, which leads to increased Y_{H_2}.

The interaction between catalyst weight and feed flow rate on H_2 production was plotted in Fig. 11d. According to Fig. 11d, maximum Y_{H_2} is obtained at lower catalyst weight (~0.3 g) and slightly high feed flow rate. This occurs due to the reason that a higher feed flow rate causes lesser reactants contact time on the catalyst surface. Hence, incomplete steam reforming reaction is more likely to occur, thus lowering Y_{H_2}.

In Fig. 11e, the effect of interaction between feed flow rate and S/C molar ratio on H_2 production is illustrated. The H_2 production was enhanced significantly at a high S/C molar ratio since steam acts as a gasification agent that will promote the H_2 production [42]. This result inferred that the WGS side reaction accompanied the SRT reaction, which produces more H_2 and CO_2 by consuming CO [21]. Therefore, at low feed flow rate and low S/C molar ratio, the H_2 yield is decreased since the reverse WGS reaction is more likely to occur. Even though higher Y_{H_2} could be achieved at a high S/C ratio, it is not recommended because of the possibility of sintering on the active sites [97]. In addition, the involved reaction would be more of steam gasification rather than toluene reforming [42]. Thus, the optimum S/C ratio is preferred because it is more reasonable and acceptable to achieve high catalytic performance in SRT for the H_2 production.

Fig. 11f portrays the relation between S/C molar ratio and catalyst weight for H_2 production. It can be seen higher Y_{H_2} is achieved at low S/C molar ratio (~3) and slightly lower catalyst weight (~0.2 g). This finding is in agreement with previous report by Zou et al. [97] that studied the effect of S/C ratio in SRT for H_2 production. It is reported that S/C = 1 is recommended in the SRT as the optimal ratio. In fact, too high S/C ratio may also cause adverse effect on the catalytic performance, which may cause the activity of catalyst to decrease due to the adsorption saturation of steam on the surface of the catalyst [98]. High catalyst weight promotes H_2 production since more active sites are available for CO conversion with H_2O by the WGS reaction to produce CO_2 and H_2 [19]. However, it is highly preferred to minimize the catalyst weight in terms of applicability and catalyst cost in commercial scale. Hence, it can be observed that the ANN-GA model shows higher predictive accuracy and concurs with previous reports on the effect of SRT parameters for H_2 production [24].

Comparison of predictive capabilities between ANN-GA and RSM

The estimation capabilities and modelling efficiencies of the predicted ANN-GA and RSM models were statistically compared using the root mean square error (RMSE) and coefficient of determination (R^2), as in Eqs. (8) and (9), respectively, according to the following expression:

$$\mathrm{RMSE} = \left(\frac{1}{2}\sum_{i=1}^{n}\left(y_i - y_{di}\right)^2\right)^{\frac{1}{2}} \tag{8}$$

$$R^2 = 1 - \frac{\sum_{i=1}^{n}\left(y_i - y_{di}\right)^2}{\sum_{i=1}^{n}\left(y_{di} - y_m\right)^2} \tag{9}$$

Please cite this article as: Yahya HSM et al., Optimization of hydrogen production via toluene steam reforming over Ni–Co supported modified-activated carbon using ANN coupled GA and RSM, International Journal of Hydrogen Energy, https://doi.org/10.1016/j.ijhydene.2020.05.033

Table 7 – Corresponding predicted and observed response at optimum conditions obtained from ANN-GA, RSM and experiment.

Modelling technique	Process Parameter				Response: H_2 yield			Statistical values	
	X_1	X_2	X_3	X_4	Predicted	Observed	Error	R^2	RMSE
ANN-GA	700	0.034	0.1	1	93.7%	92.6%	1.19%	0.95	4.09
RSM	762	0.022	0.3	5.6	86.3%	81.4%	6.02%	0.87	6.92

where y_i is the predicted value, y_{di} is the actual value, y_m is the average of the actual values and n is the number of points. RMSE was mostly employed as a measure of differences between the observed (experimental data) and predicted values. The R^2 describes and explicates the goodness of fit between the predicted models and the experimental data. The value of R^2 close to unity indicates a good fit of the data by the predicted models.

The statistical values of R^2 and RMSE of both models represented in Table 7 confirmed the higher prediction accuracy and efficiency of ANN-GA prediction compared to RSM model for H_2 yield. This can be seen by the higher R^2 value of the ANN-GA model (0.95) than RSM (0.87), which demonstrated the superiority of the ANN-GA model in terms of predictive and estimation capabilities. As for the statistical error value comparison, lower value of RMSE was obtained by ANN-GA with 4.09% prediction error compared to that of RSM with 6.92% suggest that the ANN-GA model possesses better prediction and generalization characteristics to the experimental data. A similar trend has been reported by various authors related to process optimization for various reaction including steam reforming [46,67,99,100]. Higher predictive accuracy of the ANN-GA model is attributed to the universal ability of ANN-GA to estimate the nonlinearity behavior of the system, while the RSM model is constrained to the second-order polynomial regression [50]. Hence, these results establish the advantage of ANN-GA model can be used in the prediction of the H_2 yield as an alternative to the RSM.

Next, the optimum conditions for the H_2 production from SRT over Ni–Co/ACP catalyst were predicted using ANN-GA and RSM models. Table 7 summarizes the maximum predicted value ofY_{H_2}, its predicted value of optimum SRT conditions and the observed experimental values obtained for both models. It can be observed that both models predicted a similar value for the optimum reaction temperature of higher than 700 °C. These findings coincide with the previous study reported by Ayodele et al. [100], where high Y_{H_2} was achieved with the increase in temperature attributed by the Arrhenius behavior in steam reforming as a temperature-dependent chemical reaction. The predicted percentage error of Y_{H_2} is 1.19% and 6.02% for ANN-GA and RSM models, respectively. These results suggest greater accuracy and higher reliability of ANN-GA in modelling and optimizing the SRT parameter interaction related to the SRT reaction for H_2 production. ANN-GA model employs various sigmoid transfer functions in the simulation of the complex nonlinear interactions between the process input and output variables of the SRT. On the other hand, RSM has limitations in reliably modelling the multifaceted behavior of the steam reforming process. In addition, the predominance of ANN over RSM as a predictive steam reforming modelling tool has been reported by Jha et al. [67].

The performance of ANN-GA and RSM models are further evaluated by comparing the predicted and experimental values of H_2 yield generated via SRT over the synthesized Ni–Co/ACP catalyst (Fig. 12). It can be seen from Fig. 12a that high conformity and correlation exist between the experimental and predicted data for each experimental run of the DOE in the linear fit comparison. The ANN-GA model possesses higher accuracy than the RSM because the curve of the ANN-GA predicted values are closer to the experimental data compared to RSM predicted values [70]. The closer the curve of predicted data to the experimental data, the higher the accuracy of the model. Fig. 12b displays the comparative parity plot of the model predicted values obtained from RSM and ANN for the design of experiments. The ANN-GA model predictions are much closer to the line of the perfect prediction than the RSM model, indicating that the ANN-GA model possesses higher predictive accuracy than RSM.

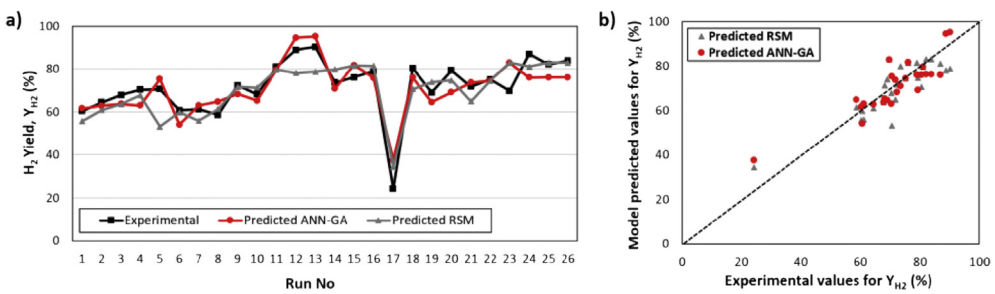

Fig. 12 – (a) Linear fit comparison; and (b) Parity plot of predicted RSM and ANN-GA values vs. experimental values of H_2 yield (%) in SRT over Ni–Co/ACP catalyst for each experimental run.

Please cite this article as: Yahya HSM et al., Optimization of hydrogen production via toluene steam reforming over Ni–Co supported modified-activated carbon using ANN coupled GA and RSM, International Journal of Hydrogen Energy, https://doi.org/10.1016/j.ijhydene.2020.05.033

Conclusions

A comparative assessment between ANN-GA and RSM model for the optimization of H_2 production via catalytic SRT using the synthesized Ni–Co supported on modified-AC catalyst has been established. Process parameters namely temperature, feed flow rate, catalyst weight and steam-to-carbon ratio are optimized using RSM and ANN-GA models. The ANOVA and response surface plot in RSM confirm that temperature is the most significant parameter in SRT for maximum H_2 yield. The interaction effects in ANN models display higher prediction accuracy than RSM. The developed ANN model exhibits a good correlation on the validation of experiments. The best network structure of 4-14-1 is utilized in GA optimization. The statistical parameter comparison infers that ANN-GA model has greater accuracy and higher reliability since it is able to capture the nonlinearities of experimental data with higher R^2 and lower RMSE. Hence, ANN-GA model is a potential alternative to RSM for modelling, predicting and optimizing H_2 production from catalytic SRT with better predictive capability.

Acknowledgement

The authors would like to thank Universiti Teknologi Malaysia and the Ministry of Higher Education, Malaysia for the financial support received through the Tier 1 Research University Grant Scheme (Vot 17H09) and Fundamental Research Grant Scheme-Malaysia Research Star Award (FRGS-MRSA), Vot 4F988. The assistance by the University Industry Research Laboratory (UIRL) and Analytical Laboratory of School of Chemical and Energy Engineering, Faculty of Engineering, Universiti Teknologi Malaysia for characterization and analytical parts are also appreciated.

REFERENCES

[1] Li S, Zheng H, Zheng Y, Tian J, Jing T, Chang JS, et al. Recent advances in hydrogen production by thermo-catalytic conversion of biomass. Int J Hydrogen Energy 2019;44(28):14266–78.
[2] The Future of Hydrogen: seizing today's opportunities - report prepared by the IEA for the G20, Japan. International Energy Agency; 2019.
[3] Baykara SZ. Hydrogen: a brief overview on its sources, production and environmental impact. Int J Hydrogen Energy 2018;43(23):10605–14.
[4] Rios MLV, Gonzalez AM, Lora EES, del Olmo OAA. Reduction of tar generated during biomass gasification: a review. Biomass Bioenergy 2018;108:345–70.
[5] Tan RS, Abdullah TAT, Mahmud SA, Zin RM, Isa KM. Catalytic steam reforming of complex gasified biomass tar model toward hydrogen over dolomite promoted nickel catalysts. Int J Hydrogen Energy 2019;44(39):21303–14.
[6] Guan GQ, Kaewpanha M, Hao XG, Abudula A. Catalytic steam reforming of biomass tar: prospects and challenges. Renew Sustain Energy Rev 2016;58:450–61.
[7] Zhang ZK, Liu LN, Shen BX, Wu CF. Preparation, modification and development of Ni-based catalysts for catalytic reforming of tar produced from biomass gasification. Renew Sustain Energy Rev 2018;94:1086–109.
[8] Martono E, Hyman MP, Vohs JM. Reaction pathways for ethanol on model Co/ZnO(0001) catalysts. Phys Chem Chem Phys 2011;13(20):9880–6.
[9] Benito M, Ortiz I, Rodríguez L, Muñoz G. Ni–Co bimetallic catalyst for hydrogen production in sewage treatment plants: biogas reforming and tars removal. Int J Hydrogen Energy 2015;40(42):14456–68.
[10] Sharma YC, Kumar A, Prasad R, Upadhyay SN. Ethanol steam reforming for hydrogen production: latest and effective catalyst modification strategies to minimize carbonaceous deactivation. Renew Sustain Energy Rev 2017;74:89–103.
[11] Takise K, Manabe S, Muraguchi K, Higo T, Ogo S, Sekine Y. Anchoring effect and oxygen redox property of Co/$La_{0.7}Sr_{0.3}AlO_{3-\delta}$ perovskite catalyst on toluene steam reforming reaction. Appl Catal Gen 2017;538:181–9.
[12] Kumar A, Singh R, Sinha ASK. Catalyst modification strategies to enhance the catalyst activity and stability during steam reforming of acetic acid for hydrogen production. Int J Hydrogen Energy 2019;44:12983–3010.
[13] Oemar U, Ang ML, Hidajat K, Kawi S. Enhancing performance of Ni/La_2O_3 catalyst by Sr-modification for steam reforming of toluene as model compound of biomass tar. RSC Adv 2015;5(23):17834–42.
[14] Gao NB, Han Y, Quan C. Study on steam reforming of coal tar over Ni-Co/ceramic foam catalyst for hydrogen production: effect of Ni/Co ratio. Int J Hydrogen Energy 2018;43(49):22170–86.
[15] Higo T, Saito H, Ogo S, Sugiura Y, Sekine Y. Promotive effect of Ba addition on the catalytic performance of Ni/$LaAlO_3$ catalysts for steam reforming of toluene. Appl Catal Gen 2017;530:125–31.
[16] Koike M, Li D, Watanabe H, Nakagawa Y, Tomishige K. Comparative study on steam reforming of model aromatic compounds of biomass tar over Ni and Ni–Fe alloy nanoparticles. Appl Catal Gen 2015;506:151–62.
[17] Koike M, Hisada Y, Wang L, Li D, Watanabe H, Nakagawa Y, et al. High catalytic activity of Co-Fe/α-Al_2O_3 in the steam reforming of toluene in the presence of hydrogen. Appl Catal B Environ 2013;140–141:652–62.
[18] Wang L, Li D, Koike M, Watanabe H, Xu Y, Nakagawa Y, et al. Catalytic performance and characterization of Ni–Co catalysts for the steam reforming of biomass tar to synthesis gas. Fuel 2013;112:654–61.
[19] Abbas T, Tahir M, Saidina Amin NA. Enhanced metal–support interaction in Ni/Co_3O_4/TiO_2 nanorods toward stable and dynamic hydrogen production from phenol steam reforming. Ind Eng Chem Res 2018;58(2):517–30.
[20] Nabgan W, Abdullah TAT, Mat R, Nabgan B, Triwahyono S, Ripin A. Hydrogen production from catalytic steam reforming of phenol with bimetallic nickel-cobalt catalyst on various supports. Appl Catal Gen 2016;527:161–70.
[21] Li ZW, Li M, Ashok J, Sibudjing K. NiCo@NiCo phyllosilicate@CeO_2 hollow core shell catalysts for steam reforming of toluene as biomass tar model compound. Energy Convers Manag 2019;180:822–30.
[22] Tan RS, Abdullah TAT, Ripin A, Ahmad A, Isa KM. Hydrogen-rich gas production by steam reforming of gasified biomass tar over Ni/dolomite/La_2O_3 catalyst. J Environ Chem Eng 2019;7(6):103490.
[23] Meng J, Zhao Z, Wang X, Chen J, Zheng A, Huang Z, et al. Steam reforming and carbon deposition evaluation of phenol and naphthalene used as tar model compounds over Ni and Fe olivine-supported catalysts. J Energy Inst 2019;92(6):1765–78.

Please cite this article as: Yahya HSM et al., Optimization of hydrogen production via toluene steam reforming over Ni–Co supported modified-activated carbon using ANN coupled GA and RSM, International Journal of Hydrogen Energy, https://doi.org/10.1016/j.ijhydene.2020.05.033

[24] Meng J, Zhao Z, Wang X, Wu X, Zheng A, Huang Z, et al. Effects of catalyst preparation parameters and reaction operating conditions on the activity and stability of thermally fused Fe-olivine catalyst in the steam reforming of toluene. Int J Hydrogen Energy 2018;43(1):127–38.
[25] He L, Hu S, Jiang L, Liao G, Chen X, Han H, et al. Carbon nanotubes formation and its influence on steam reforming of toluene over Ni/Al_2O_3 catalysts: roles of catalyst supports. Fuel Process Technol 2018;176:7–14.
[26] de Castro TP, Silveira EB, Rabelo-Neto RC, Borges LEP, Noronha FB. Study of the performance of Pt/Al_2O_3 and $Pt/CeO_2/Al_2O_3$ catalysts for steam reforming of toluene, methane and mixtures. Catal Today 2018;299:251–62.
[27] Zhang T, Liu Z, Zhu Y-A, Liu Z, Sui Z, Zhu K, et al. Dry reforming of methane on Ni-Fe-MgO catalysts: influence of Fe on carbon-resistant property and kinetics. Appl Catal B Environ 2020;264:118497.
[28] Ravenni G, Sárossy Z, Ahrenfeldt J, Henriksen UB. Activity of chars and activated carbons for removal and decomposition of tar model compounds – a review. Renew Sustain Energy Rev 2018;94:1044–56.
[29] Matos I, Bernardo M, Fonseca I. Porous carbon: a versatile material for catalysis. Catal Today 2017;285:194–203.
[30] Liu XJ, Yang XQ, Liu C, Chen P, Yue XM, Zhang SQ. Low-temperature catalytic steam reforming of toluene over activated carbon supported nickel catalysts. J Taiwan Inst Chem E 2016;65:233–41.
[31] Gallegos-Suarez E, Guerrero-Ruiz A, Rodriguez-Ramos I. Efficient hydrogen production from glycerol by steam reforming with carbon supported ruthenium catalysts. Carbon 2016;96:578–87.
[32] Barthos R, Solymosi F. Hydrogen production in the decomposition and steam reforming of methanol on Mo_2C/carbon catalysts. J Catal 2007;249(2):289–99.
[33] Li L, Meng B, Qin X, Yang Z, Chen J, Yan K, et al. Toluene microwave cracking and reforming over bio-char with in-situ activation and ex-situ impregnation of metal. Renew Energy 2020;149:1205–13.
[34] Shen Y. Chars as carbonaceous adsorbents/catalysts for tar elimination during biomass pyrolysis or gasification. Renew Sustain Energy Rev 2015;43:281–95.
[35] Lam E, Luong JHT. Carbon materials as catalyst supports and catalysts in the transformation of biomass to fuels and chemicals. ACS Catal 2014;4(10):3393–410.
[36] Daud WMAW, Houshamnd AH. Textural characteristics, surface chemistry and oxidation of activated carbon. J Nat Gas Chem 2010;19(3):267–79.
[37] Sun Y, Zhang G, Xu Y, Zhang R. Catalytic performance of dioxide reforming of methane over Co/AC-N catalysts: effect of nitrogen doping content and calcination temperature. Int J Hydrogen Energy 2019;44(31):16424–35.
[38] Shen BX, Liu Z, Xu H, Wang FM. Enhancing the absorption of elemental mercury using hydrogen peroxide modified bamboo carbons. Fuel 2019;235:878–85.
[39] Shen C, Zhou W, Yu H, Du L. Ni nanoparticles supported on carbon as efficient catalysts for steam reforming of toluene (model tar). Chin J Chem Eng 2018;26(2):322–9.
[40] Li Q, Wang Q, Kayamori A, Zhang JS. Experimental study and modeling of heavy tar steam reforming. Fuel Process Technol 2018;178:180–8.
[41] Ghosal PS, Kattil KV, Yadav MK, Gupta AK. Adsorptive removal of arsenic by novel iron/olivine composite: insights into preparation and adsorption process by response surface methodology and artificial neural network. J Environ Manag 2018;209:176–87.
[42] Xiao XB, Liu J, Gao AN, Zhouyu MQ, Liu BH, Gao MD, et al. The performance of nickel-loaded lignite residue for steam reforming of toluene as the model compound of biomass gasification tar. J Energy Inst 2018;91(6):867–76.
[43] Dantas TNC, Cabral TJO, Neto AAD, Moura MCPA. Enrichment of patchoulol extracted from patchouli (Pogostemon cablin) oil by molecular distillation using response surface and artificial neural network models. J Ind Eng Chem 2020;81:219–27.
[44] Li S, Qin X, Zhang G, Xu Y, Lv Y. Optimization of content of components over activated carbon catalyst on CO_2 reforming of methane using multi-response surface methodology. Int J Hydrogen Energy 2020;45(16):9695–709.
[45] Jacob J, Shanmugavelu P, Balasubramaniam R. Investigation of the performance of 248 nm excimer laser assisted photoresist removal process in gaseous media by response surface methodology and artificial neural network. J Manuf Process 2019;38:516–29.
[46] Esonye C, Onukwuli OD, Ofoefule AU. Optimization of methyl ester production from Prunus Amygdalus seed oil using response surface methodology and Artificial Neural Networks. Renew Energy 2019;130:61–72.
[47] Rezaei R, Moradi G, Sharifnia S. Dry reforming of methane over $Ni-Cu/Al_2O_3$ catalyst coatings in a microchannel reactor: modeling and optimization using design of experiments. Energy Fuels 2019;33(7):6689–706.
[48] Selvaraj S, Vytla RM, Vijay GS, Natarajan K. Modeling and optimization of tannase production with Triphala in packed bed reactor by response surface methodology, genetic algorithm, and artificial neural network. 3 Biotech 2019;9(7):259.
[49] Aghbashlo M, Tabatabaei M, Rastegari H, Ghaziaskar HS, Valijanian E. Exergy-based optimization of a continuous reactor applied to produce value-added chemicals from glycerol through esterification with acetic acid. Energy 2018;150:351–62.
[50] Kim Z, Shin Y, Yu J, Kim G, Hwang S. Development of NO_x removal process for LNG evaporation system: comparative assessment between response surface methodology (RSM) and artificial neural network (ANN). J Ind Eng Chem 2019;74:136–47.
[51] Rahman RO Abdel, Moamen OA Abdel, Abdelmonem N, Ismail IM. Optimizing the removal of strontium and cesium ions from binary solutions on magnetic nano-zeolite using response surface methodology (RSM) and artificial neural network (ANN). Environ Res 2019;173:397–410.
[52] Zhao F, Lu J, Jin X, Wang Z, Sun Y, Gao D, et al. Comparison of response surface methodology and artificial neural network to optimize novel ophthalmic flexible nano-liposomes: characterization, evaluation, in vivo pharmacokinetics and molecular dynamics simulation. Colloids Surf B Biointerfaces 2018;172:288–97.
[53] Kumar GS, Reddy BV, Sankaraiah G, Reddy PV. Modeling the performance of vortex tube using response surface methodology and artificial neural networks. IOP Conf Ser Mater Sci Eng 2018;390(1):12010.
[54] Bezerra MA, Santelli RE, Oliveira EP, Villar LS, Escaleira LA. Response surface methodology (RSM) as a tool for optimization in analytical chemistry. Talanta 2008;76(5):965–77.
[55] Aggarwal CC. Neural networks and deep learning. USA: Springer International Publishing; 2018.
[56] Ghasemzadeh K, Ahmadnejad F, Aghaeinejad-Meybodi A, Basile A. Hydrogen production by a Pd-Ag membrane reactor during glycerol steam reforming: ANN modeling study. Int J Hydrogen Energy 2018;43(15):7722–30.
[57] Chiroma H, Noor ASM, Abdulkareem S, Abubakar AI, Hermawan A, Qin H, et al. Neural networks optimization through genetic algorithm searches: a review. Appl Math Inform Sci 2017;11(6):1543–64.

Please cite this article as: Yahya HSM et al., Optimization of hydrogen production via toluene steam reforming over Ni–Co supported modified-activated carbon using ANN coupled GA and RSM, International Journal of Hydrogen Energy, https://doi.org/10.1016/j.ijhydene.2020.05.033

[58] Cifuentes B, Figueredo M, Cobo M. Response surface methodology and aspen plus integration for the simulation of the catalytic steam reforming of ethanol. Catalysts 2017;7(1):15.
[59] Sidik SM, Triwahyono S, Jalil AA, Majid ZA, Salamun N, Talib NB, et al. CO_2 reforming of CH_4 over Ni–Co/MSN for syngas production: role of Co as a binder and optimization using RSM. Chem Eng J 2016;295:1–10.
[60] Senseni AZ, Fattahi SMS, Rezaei M, Meshkani F. A comparative study of experimental investigation and response surface optimization of steam reforming of glycerol over nickel nano-catalysts. Int J Hydrogen Energy 2016;41(24):10178–92.
[61] Azaman F, Azid A, Juahir H, Mohamed M, Yunus K, Toriman ME, et al. Application of artificial neural network and response surface methodology for modelling of hydrogen production using nickel loaded zeolite. J Teknol 2015;77(1):109–18.
[62] Awalludin MF, Sulaiman O, Hashim R, Nadhari WNAW. An overview of the oil palm industry in Malaysia and its waste utilization through thermochemical conversion, specifically via liquefaction. Renew Sustain Energy Rev 2015;50:1469–84.
[63] Daud WMAW, Ali WSW. Comparison on pore development of activated carbon produced from palm shell and coconut shell. Bioresour Technol 2004;93(1):63–9.
[64] Morin M, Nitsch X, Pecate S, Hemati M. Tar conversion over olivine and sand in a fluidized bed reactor using toluene as model compound. Fuel 2017;209:25–34.
[65] Montgomery DC. Design and analysis of experiments. 8th ed. John Wiley & Sons, Inc.; 2013.
[66] Myers RH, Montgomery DC, Anderson-Cook CM. Response surface methodology: process and product optimization using designed experiments. 3rd ed. New Jersey: John Wiley & Sons, Inc.; 2009.
[67] Jha P, Kana EBG, Schmidt S. Can artificial neural network and response surface methodology reliably predict hydrogen production and COD removal in an UASB bioreactor? Int J Hydrogen Energy 2017;42(30):18875–83.
[68] Ramli NAS, Ya'aini N, Amin NAS. Comparison of response surface methodology and artificial neural network for optimum levulinic acid production from glucose, empty fruit bunch and kenaf. Int J Nano Biomaterials 2014;5(1):59–74.
[69] Shin Y, Kim Z, Yu J, Kim G, Hwang S. Development of NO_x reduction system utilizing artificial neural network (ANN) and genetic algorithm (GA). J Clean Prod 2019;232:1418–29.
[70] Nasrudin NA, Jewaratnam J, Hossain A, Ganeson PB. Performance comparison of feedforward neural network training algorithms in modelling microwave pyrolysis of oil palm fibre for hydrogen and biochar production. Asia Pac J Chem Eng 2019;15(1):e2388.
[71] Shahbaz M, Taqvi SA, Loy ACM, Inayat A, Uddin F, Bokhari A, et al. Artificial neural network approach for the steam gasification of palm oil waste using bottom ash and CaO. Renew Energy 2019;132:243–54.
[72] Talebian-Kiakalaieh A, Amin NAS, Zarei A, Noshadi I. Transesterification of waste cooking oil by heteropoly acid (HPA) catalyst: optimization and kinetic model. Appl Energy 2013;102:283–92.
[73] Kasmuri NH, Kamarudin SK, Abdullah SRS, Hasan HA, Som AM. Integrated advanced nonlinear neural network-simulink control system for production of bio-methanol from sugar cane bagasse via pyrolysis. Energy 2019;168:261–72.
[74] Sydney EB, Duarte ER, Burgos WJM, de Carvalho JC, Larroche C, Soccol CR. Development of short chain fatty acid-based artificial neuron network tools applied to biohydrogen production. Int J Hydrogen Energy 2019;45(8):5175–81.
[75] Magrab EB, Azarm S, Balachandran B, Duncan JH, Herold KE, Walsh GC. An engineer's guide to MATLAB with applications from mechanical, aerospace, electrical, civil, and biological systems engineering. New Jersey: Prentice Hall; 2013.
[76] Lopez CP. MATLAB optimization techniques. Apress; 2014.
[77] Istadi, Amin NAS. Optimization of process parameters and catalyst compositions in carbon dioxide oxidative coupling of methane over CaO–MnO/CeO_2 catalyst using response surface methodology. Fuel Process Technol 2006;87(5):449–59.
[78] Warhurst AM, Fowler GD, McConnachie GL, Pollard SJT. Pore structure and adsorption characteristics of steam pyrolysis carbons from Moringa oleifera. Carbon 1997;35(8):1039–45.
[79] Oh G, Park SY, Seo MW, Kim YK, Ra HW, Lee J-G, et al. Ni/Ru–Mn/Al_2O_3 catalysts for steam reforming of toluene as model biomass tar. Renew Energy 2016;86:841–7.
[80] Sing KSW, Everett DH, Haul RAW, Moscou L, Pierotti RA, Rouquerol J, et al. Reporting physisorption data for gas solid systems with special reference to the determination of surface-area and porosity (recommendations 1984). Pure Appl Chem 1985;57(4):603–19.
[81] Laksaci H, Khelifi A, Trari M, Addoun A. Synthesis and characterization of microporous activated carbon from coffee grounds using potassium hydroxides. J Clean Prod 2017;147:254–62.
[82] Rouquerol J, Rouquerol F, Llewellyn P, Maurin G, Sing KS. Adsorption by powders and porous solids: principles, methodology and applications. Academic press; 2013.
[83] Pastor-Pérez L, Sepúlveda-Escribano A. Multicomponent NiSnCeO_2/C catalysts for the low-temperature glycerol steam reforming. Appl Catal Gen 2017;529:118–26.
[84] Qian KZ, Kumar A. Catalytic reforming of toluene and naphthalene (model tar) by char supported nickel catalyst. Fuel 2017;187:128–36.
[85] Huang L, Lv Y, Wu S, Liu P, Xiong W, Hao F, et al. Activated carbon supported bimetallic catalysts with combined catalytic effects for aromatic nitro compounds hydrogenation under mild conditions. Appl Catal Gen 2019;577:76–85.
[86] Pastor-Pérez L, Buitrago-Sierra R, Sepúlveda-Escribano A. CeO_2-promoted Ni/activated carbon catalysts for the water–gas shift (WGS) reaction. Int J Hydrogen Energy 2014;39(31):17589–99.
[87] Chen Y, Zhang X, Zhang H, Sun X, Zhang D, Ma Y. High-performance supercapacitors based on a graphene–activated carbon composite prepared by chemical activation. RSC Adv 2012;2(20):7747–53.
[88] Huang X, Ji C, Wang C, Xiao F, Zhao N, Sun N, et al. Ordered mesoporous CoO-NiO-Al_2O_3 bimetallic catalysts with dual confinement effects for CO_2 reforming of CH_4. Catal Today 2017;281:241–9.
[89] Al-Fatesh AS, Arafat Y, Atia H, Ibrahim AA, Ha QLM, Schneider M, et al. CO_2-reforming of methane to produce syngas over Co-Ni/SBA-15 catalyst: effect of support modifiers (Mg, La and Sc) on catalytic stability. J CO2 Util 2017;21:395–404.
[90] Mate VR, Jha A, Joshi UD, Patil KR, Shirai M, Rode CV. Effect of preparation parameters on characterization and activity of Co_3O_4 catalyst in liquid phase oxidation of lignin model substrates. Appl Catal A Gen 2014;487:130–8.

Please cite this article as: Yahya HSM et al., Optimization of hydrogen production via toluene steam reforming over Ni–Co supported modified-activated carbon using ANN coupled GA and RSM, International Journal of Hydrogen Energy, https://doi.org/10.1016/j.ijhydene.2020.05.033

[91] Xiao F, Jiao G, Shen H, Li K, Ouyang Y, Zhang W, et al. Influences of pretreatment of carbon on performance of carbon supported Pd nanocatalyst for nitrobenzene hydrogenation. J Nanosci Nanotechnol 2020;20(1):629–35.
[92] Sarafraz MM, Safaei MR, Goodarzi M, Arjomandi M. Experimental investigation and performance optimisation of a catalytic reforming micro-reactor using response surface methodology. Energy Convers Manag 2019;199:111983.
[93] Basu S, Pradhan NC. Steam reforming of acetone over NiCoMgAl mixed oxide catalysts obtained from hydrotalcite precursors. Int J Hydrogen Energy 2019. In press.
[94] Ebshish A, Yaakob Z, Taufiq-Yap YH, Bshish A. Investigation of the process conditions for hydrogen production by steam reforming of glycerol over Ni/Al_2O_3 catalyst using response surface methodology (RSM). Materials 2014;7(3):2257–72.
[95] Zamzuri NH, Mat R, Amin NAS, Talebian-Kiakalaieh A. Hydrogen production from catalytic steam reforming of glycerol over various supported nickel catalysts. Int J Hydrogen Energy 2017;42(14):9087–98.
[96] Biglarijoo N, Mirbagheri SA, Bagheri M, Ehteshami M. Assessment of effective parameters in landfill leachate treatment and optimization of the process using neural network, genetic algorithm and response surface methodology. Process Saf Environ Protect 2017;106:89–103.
[97] Zou XH, Chen TH, Zhang P, Chen D, He JK, Dang YL, et al. High catalytic performance of Fe-Ni/Palygorskite in the steam reforming of toluene for hydrogen production. Appl Energy 2018;226:827–37.
[98] Swierczynski D, Libs S, Courson C, Kiennemann A. Steam reforming of tar from a biomass gasification process over Ni/olivine catalyst using toluene as a model compound. Appl Catal B Environ 2007;74(3–4):211–22.
[99] Sun Y, Yang G, Wen C, Zhang L, Sun Z. Artificial neural networks with response surface methodology for optimization of selective CO_2 hydrogenation using K-promoted iron catalyst in a microchannel reactor. J CO_2 Util 2018;24:10–21.
[100] Ayodele BV, Khan MR, Nooruddin SS, Cheng CK. Modelling and optimization of syngas production by methane dry reforming over samarium oxide supported cobalt catalyst: response surface methodology and artificial neural networks approach. Clean Technol Environ Policy 2017;19(4):1181–93.

Please cite this article as: Yahya HSM et al., Optimization of hydrogen production via toluene steam reforming over Ni–Co supported modified-activated carbon using ANN coupled GA and RSM, International Journal of Hydrogen Energy, https://doi.org/10.1016/j.ijhydene.2020.05.033